INVESTIGATION OF THE ADSORPTION OF BIOMOLECULES USING SURFACE PLASMON FLUORESCENCE SPECTROSCOPY AND MICROSCOPY

NIU LIFANG

(Department of Chemistry, NUS)

A THESIS SUBMITTED

FOR THE DEGREE OF MASTER OF SCIENCE

DEPARTMENT OF CHEMISTRY SCIENCE

NATIONAL UNIVERSITY OF SINGAPORE

2004

Acknowledgements

This work was done with the help and instructions of many colleagues and friends, and it is my pleasure to acknowledge their contribution. I’d like to give my greatest respects to my two supervisors, Prof. Wolfgang Knoll and Dr. Thorsten Wohland, for their always passionate support to this work. I am also grateful for many enlightening discussions with Dr. Evelyne Schmid and Dr. Rudolf Robelek.

CONTENTS

Summary

The development and characterization of biomolecule sensor formats based on the optical technique Surface Plasmon Resonance (SPR) Spectroscopy were investigated. The study can be divided into two parts of different scope: In the first part the working mechanism and typical experiments of Surface-plamon Field Enhanced Spectroscopy (SPFS) were studied. In the second part the ideas were extended to the development of fluorescence spectrometry and microscope formats.

Fluorescence molecules could be excited in the evanescent surface plasmon field near the surface. The fluorescence emission mediated by plasmon excitation was characterized. DNA hybridizing could be monitored on metallic surfaces using SPFS. The sensor architecture consisted of an unlabelled oligonucleotide probe sequence immobilized on streptavidin matrix. Cy3 and Cy5 labeled target sequences were hybridized from solution and their fluorescence signals were recorded. The high surface sensitivity of fluorescence technique coupled to surface plasmon resonance permitted the real-time recording of hybridization kinetics.

On the basis of the investigations in Surface-plamon Field Enhanced Spectroscopy (SPFS), new novel detection schemes for labeled targets were developed. The first one is a SPR fluorescence imaging format. Patterned self assembled monolayers (SAMs) were prepared and used to direct the spatial distribution of biomolecules immobilized on surfaces. Here the patterned monolayers serve as molecular templates to detect different biomolecules to pre-determined locations on a surface. The binding processes of labeled target biomolecules from solution to the sensor surface were visually and kinetically recorded by fluorescence microscope, in which fluorescence was excited by the evanescent field of propagating plasmon surface polaritons. The

second format which also originates from the SPFS technique concerns the coupling of fluorometry to a normal SPR setup. A spectrograph mounted in place of the photomultiplier or microscope can provide the information about the fluorescence spectrum as well as the fluorescence intensity.

The final study demonstrates an analytical combination of surface plasmon enhanced fluorescence spectroscopy, microscopy and spectrometry with fluorescent ananlytes tagged by semiconducting nanocrystals (quantum dots). These quantum dots show several advantages compared to the classic organic dyes, the biggest one being their broad spectral absorption range and the well defined sharp emission wavelength, which makes it possible to excite several quantum dot populations simultaneously with a single light source and, hence, at a single angle of incidence for resonant surface plasmon excitation.

Our experiments showed clearly, that the specific hybridization of QD conjugated DNA-single stands to sensor attached complementary sequences could be detected by a substantial shift in the angular reflectivity spectrum of the SPR, as well as, by a high fluorescence signal, originating from the DNA bound QDs.

The transfer of the system to the platform of surface plasmon enhanced fluorescence microscopy and the organization of the catcher probe DNA in a micro array format rendered a qualitative analytical approach of measuring the decomposition of QDx-DNAy mixtures possible. The spectral resolution of the obtained multicolor images with a spectrograph shows the potential of the combination of QD-DNA conjugates with SPFS for future applications in DNA chip analytics.

LIST OF TABLES:

LIST OF FIGURES:

1 Introduction

The study of biomolecular interactions and recognition processes are an important topic in the field of biophysics. They are central to our understanding of vital biological phenomena such as immunologic reactions and signal transduction. In addition, these biological recognition reactions are at the heart of the development and application of biosensors. A number of analytical techniques used in biology, medicine and pharmacy have been developed over the past years. Novel detection methods have been developed which combine the specificity of biomolecular recognitions systems with the advantages of instrumental analysis. Biosensor devices have gained importance in areas like medical diagnostic, quality control and environmental analysis.

Biosensor

A biosensor is defined as an analytical device which contains a biological recognition element immobilized on a solid surface and an transduction element which converts analyte binding events to a measurable signal[1-2]. Biosensors use the highly specific recognition properties of biological molecules, to detect the presence of binding partners, usually at extremely low concentrations. Biological recognition can surpass any man-made concepts in sensitivity and specificity. This specificity permits very similar analytes to be distinguished from each other by their interaction with immobilized bio-molecules (antibodies, enzymes or nucleic acids). Biosensors are valuable tools for fast and reliable detection of ananytes and have reached an importance for scientific, bio-medical and pharmaceutical applications [3-4]. The advantages that are offered by the ideal biosensor over other forms of analytical techniques are: the high sensitivity and selectivity, low detection limit, good

reproducibility, rapid response, reusability of devices, ease of fabrication and application, possibility of miniaturization, ruggedness and low fabrication cost. By immobilizing the bio-recognition element on the sensor surface one gains the advantage of reusability of the device due to the ease of separating bound and unbound species. By simple washing steps the non-specifically bound molecules may be removed. Some surface sensitive detection formats, such as evanescent wave techniques, even make these washing steps redundant. These techniques are relatively insensitive to the presence of analytes in the bulk solution.

The mere presence of the analyte itself does not cause any measurable signal from the sensor, but the selective binding of the analyte of interest to the biological component. The latter is coupled to a transducer, which responds the binding of the bio-molecule. [5-6]. The three most frequently used transduction devices are electrochemical, piezoelectric and optical detectors. While electrochemical sensors respond to changes in the ionic concentration, redox potential, electron transfer rate or electron density upon analyte binding, piezoelectric sensors monitor changes in the adsorbed mass on the sensor surface [7]. A large number of optical biosensors are based on the principles of fluorescence, chemi-luminescence or absorption spectroscopy.

Surface-sensitive techniques

Surface-sensitive techniques provide a vital link, both for the understanding of biomolecular recognition and the development of biosensors. Indeed, surfaces and cell surfaces in particular, are involved in many important biological functions via the cell surface itself (the recognition of foreign molecules by specific receptors located on the cell surface for example) or across the cell membrane (as in the signal

transduction from one neuron to another involving complex membrane receptor proteins). These interfaces are central to a variety of biochemical and biophysical processes: triggering of cellular response by neurotransmitter binding, blood coagulation by foreign substances, cellular mobility, etc.

In parallel, surface-sensitive techniques bring an inherent advantage over bulk techniques in that they provide real-time binding data. By immobilizing one of the partners of the binding process on the surface of the transducer, the binding of the complement can be followed unperturbed by the presence of free molecules in the bulk. This eliminates the need for lengthy and perturbing separation steps that are required in most bulk techniques.

The techniques that provide surface-sensitivity, as well as being non-destructive and giving in-situ responses can be classified by the method of detection on which they are based:

-electrical: impedance spectroscopy
microphysiometry

-acoustic: piezoelectric waveguides

-optical: ellipsometry
reflectometric interference spectroscopy
attenuated total internal reflection infrared spectroscopy
surface plasmon resonance
total internal reflection fluorescence
optical waveguides

Evanescent Wave Sensors

Evanescent wave sensors exploit the properties of light totally reflecting at an interface and the presence of an evanescent field of light at this interface. These techniques make use of the exponentially decaying electromagnetic field at the boundary between two media of different optical constants upon irradiation with electromagnetic waves. Under total internal reflection conditions the decay length of the evanescent field into the optically thinner medium is on the order of the wavelength of the used excitation light. For visible light the field decays within a few hundred nanometers. Only analyte molecules in the evanescent region are probed, which causes the surface sensitive character of such methods. Basically, three different evanescent wave formats are known: planar waveguides, fiber-optics and surface plasmon resonance devices.

A waveguide consists of a planar glass surface with a refractive index higher than the adjacent medium. Under certain conditions light coupled into this waveguide can travel through the sample by total internal reflection. An evanescent field can interact with molecules in the region surrounding the waveguide. Adsorbed analytes change the optical properties of the waveguide and alter the boundary conditions for guiding light in the sample. Hence, the light coupling out of the waveguide can then used to monitor binding reactions at the surface of the waveguide. Fiber-optic sensors utilize the same principle as waveguides, but differ in the experimental geometry.

Surface Plasmon Resonance

The evanescent light wave is used to excite the nearly free electron gas in a thin film (~50 nm) of metal at the interface. The excitation of these so called surface plasmons, are directly dependent on the optical properties of the adjacent medium where any

mass deposition on the metal surface will lead to a change in the optical architecture, and hence, in the coupling conditions of the evanescent wave with the plasmons. The excitation of the resulting surface waves gives rise to a field enhancement compared to the intensity of the incident electromagnetic field [8]. This is used to detect mass changes on the film and thus to measure binding processes at the interface. Illumination by laser light can be used to excite the plasmons in metals. Then the system responds to changes in the optical properties of the medium close to the metal film by altering the intensity of the reflected light. For surface sensitive investigations of adsorption and desorption processes on metallic substrates Surface Plasmon Resonance is the method of choice. Commercial instruments are available (such as the BIAcore, Pharmacia, Sweden) and are routinely used to measure biomolecular interactions.

Evanescent Enhancement of Fluorescence

Generally, sensor formats can be divided into direct and indirect sensors. The first group is capable of detecting the presence of the analyte molecule directly, while the indirect schemes detect the presence of an additional signal. In electrochemistry based sensors redox-active labels like ruthenium pyridinium complexes bind to the receptor-target complex and may be detected voltammetrically. Sensitivity is an important aspect for the detection of biomolecules to improve SPR measurements. For example, the use of attached colloidal particles and amplification of hybridization signal through streptavidin have been reported. Surface Plasmon Spectroscopy (SPS) and piezo-electric techniques are sensitive to changes in the adsorbed mass and optical thickness on the surface. Labels of large molecular weight like proteins can be used to enhance the sensitivity of the system. Finally, the most prominent optical labels are fluorescent molecules. They allow for a highly sensitive detection because the

excitation and emission wavelength can be separated. Therefore fluorophores are widely used to detect molecules in a variety of applications.

The development of novel, easy-to-use detection protocols and assay designs rely on the knowledge of kinetic constants of binding reactions. Thus, surface sensitive techniques are essential for the investigation of surface reaction kinetics. Unfortunately, many of the surface sensitive techniques such as Surface Plasmon Spectroscopy lack in their detection limit if low molecular mass analytes are to be detected. Therefore, combinations of surface sensitive optical techniques with fluorescence detection formats were developed. The excitation of evanescent wave techniques has been demonstrated for waveguides and fiber-optic devices [9-11]. Fluorescent molecules close to the sensor surface are excited by the evanescent electrical field. Compared to direct illumination an enhancement of a factor of four can be reached.

Recently surface plasmons were used as intermediate states between the incident light and the excited fluorophore in Surface Plasmon Fluorescence Spectroscopy (SPFS) [12-13]. Depending on the nature of the metal the plasmon field provides the possibility to enhance the fluorescence signal up to a factor of 80. SPFS allows probing the presence of fluorescent analytes with high sensitivity and simultaneously provides information about the sensor architecture. From the viewpoint of bio-molecular architectures employed for biosensors metal surfaces are important with respect to immobilization strategies and are irreplaceable for self assembly of thiol tethered lipids, proteins and nucleic acids. The detection formats for DNA investigated in this study are based on controlled and reproducible formation of monolayers of proteins and DNA on gold and silver films. Therefore the SPFS

technique was used to characterize the formation of the supporting matrix and the DNA hybridization.

The excitation of fluorescence in the evanescent field of the plasmons is strongest close to the metal surface. On the other hand the presence of the metal can reduce the observed fluorescence intensity by inducing distance dependent quenching processes like the Förster transfer. Excitation and quenching processes exhibit different distance dependencies. An optimal distance to the metal exists at which maximal fluorescence excitation is observed. Therefore, the experimental design of the sensor surface architecture has to be optimized in order to obtain an efficient and sensitive sensor concept.

Surface plasmon field enhanced techniques are particularly suited for the study of biomolecular interactions where, in addition to its surface specificity, this technique has a very high sensitivity thanks to the possible use of efficient fluorescent labels. The use of this technique to study biomolecular recognition processes, as well as for the development of biosensors, is central to this work.

Aim of the study

The aim of this study is the development and characterization of DNA biosensor formats based on evanescent wave techniques such as Surface Plasmon Fluorescence Spectroscopy. The surface plasmon enhanced fluorescence (SPFS) set-up was recently described [13] and the current application of this technology for DNA detection on surfaces was shown. However, the fluorescence microscopy format was not investigated in full detail. Furthermore, the impact of multi-parallel biomolecular detection by SPFM and SPFS techniques on biosensor development was not evaluated. This study focuses on the development of surface plasmon enhanced fluorescence

spectroscopy (SPFS) and microscopy (SPFM) and their potential application in the field of biosensor. The aims of this study are defined as follows:

(1) Study of DNA hybridization reactions on surfaces based on SPFS.

(2) Development and characterization of novel detection formats for nucleic acids on surfaces. These studies can include the use of different fluorescence labels and different surface pattern designs.

In part 2 the theoretical background of the surface plasmon resonance techniques is reviewed and the concept of fluorescence is discussed. The combination of both techniques in the form of SPFS (spectroscopy), SPFM (microscopy), SPFS (spectrometry) and the influence of surface plasmon fields on fluorophores close to planar surfaces is discussed in part 4. The use of SPFS and SPFM for the investigation of DNA hybridization is also discussed. The design of the used sensor format is presented and the measurement principle is explained.

2 Theory

2.1 Surface Plasmon Resonance

The phenomenon of surface plasmons has been known for a long time. The underlying principles and theories are well understood, so that a number of publications can be found which discuss their properties in detail [8, 14, 15]. Surface plasmons are surface waves which can be excited at the interface between a metal and a dielectric and the exact excitation conditions strongly depend on the optical properties of the system. (Figure 2.1) It will be derived that changes in these properties will lead to altered experimental excitation conditions. This measurable response of the system permits the sensitive monitoring of processes near this interface. Numerous descriptions of successful surface plasmon based sensors can be found and are discussed later.

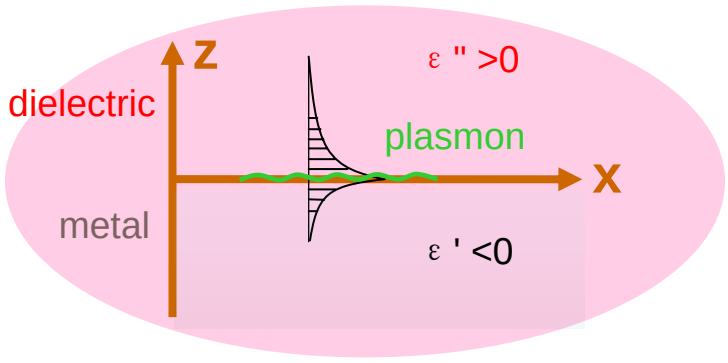

Figure 2.1: Schematic diagram of surface plasmon

A major part of this work is based on the excitation of surface waves and the interaction of the associated electromagnetic field within dielectric thin films. The theoretical background of these processes are described in detail in this chapter, since the understanding of electromagnetic waves in matter and their behavior at interfaces is essential for the following discussion. Fundamental processes like refraction,

reflection, transmission and damping of electromagnetic waves at interfaces are considered in general, followed by a discussion of surface plasmon excitation in a two layer system. Finally, the derived model will be extended to multilayer systems and the connection to experimental surface plasmon spectroscopy is made.

2.1.1. Electromagnetic Fields and Maxwell Equation of Plane Waves at interface

The general description of monochromatical electromagnetic waves in an isotropic, homogenous medium without any source terms is given by Maxwell's equations.

$$\nabla \times \mathbf{E}(\mathbf{r},t) = -\frac{\partial}{\partial t}\mathbf{B}(\mathbf{r},t) \qquad \nabla \times \mathbf{H}(\mathbf{r},t) = \frac{\partial}{\partial t}\mathbf{D}(\mathbf{r},t)$$

$$\nabla \cdot \mathbf{D}(\mathbf{r},t) = 0 \qquad \nabla \cdot \mathbf{B}(\mathbf{r},t) = 0 \tag{2.1}$$

Here, **E** is the electric field, **D** the electrical displacement, **B** the magnetic induction, **H** the magnetic field, **r** the spatial vector and t is the time. The relations between **D** and **E**, **B** and **H** are given by

$$\mathbf{D}(\mathbf{r},t) = \varepsilon\varepsilon_0\mathbf{E}(\mathbf{r},t)$$

$$\mathbf{B}(\mathbf{r},t) = \mu\mu_0\mathbf{H}(\mathbf{r},t) \tag{2.2}$$

with ε and μ being the dielectric constant and the magnetic , respectively.

The solution of the above Maxell's equations as a function of time t at point **r** is a plane wave, which can be described in a complex form as:

$$\mathbf{E}(\mathbf{r},t) = \mathbf{E}_0 \cdot \exp\left[i\left(\mathbf{k}\cdot\mathbf{r} - \omega t\right)\right] \tag{2.3}$$

The interpretation of the above equation is that only the real part of the complex quantity has a physical meaning and the orientation of $\mathbf{E}_0$ is orthogonal to **k**. For each pair of (**k**, ω) two mutually orthogonal electric field amplitudes exist, spanning the plane to give all possible polarizations. Besides the electric field, also the magnetic field (with the corresponding mathematical notation) contains the full information

about the plane wave. Both representations may be transformed into each other by use of

$$\mathbf{E}(\mathbf{r},t) = \frac{1}{\varepsilon\varepsilon_0\omega}\mathbf{k}\times\mathbf{H}(\mathbf{r},t)$$

$$\mathbf{H}(\mathbf{r},t) = \frac{1}{\mu\mu_0\omega}\mathbf{k}\times\mathbf{E}(\mathbf{r},t) \tag{2.4}$$

The dispersion equation relates the modulus $|\mathbf{k}|$ of the wavevector to a given angular frequency ω

$$\frac{\omega^2}{|\mathbf{k}|^2} = \frac{1}{\mu\mu_0\varepsilon\varepsilon_0} = \frac{c^2}{n^2} \tag{2.5}$$

Here, the refractive index n is defined as the ratio of the speed of light c in vacuum and in matter. Making the assumption of a nonmagnetic material (μ = 1) the dispersion equation can be further simplified to give

$$|\mathbf{k}| = \omega\cdot\sqrt{\varepsilon\varepsilon_0\mu\mu_0} = k_0\sqrt{\varepsilon} = k_0\cdot n \tag{2.6}$$

The situation of light passing through medium 1 with a refractive index n_1, which is then reflected at medium 2 with a refractive index n_2 that is smaller than n_1 gives rise to a special feature: Beginning at an angle of incidence θ_1 of zero the transmission angle θ_2 can be determined according to Snell's law. The increase of θ_1 leads to an increase of θ_2 up to the point where θ_2 reaches a value of 90°. Then the so-called critical angle θ_c is reached. At that point the reflectivity reaches a value of R = 1, i.e. light is totally reflected, and any further increased of θ_1 has no influence on the reflectivity anymore. However, at such high angles the component of the field normal to the surface is not longer oscillatory but decays in an exponential way as given by equation (2.1). This is the regime of evanescent waves.

2.1.2 Surface Plasmon

Before moving on to the theoretical description of plasmon surface polaritons, or surface plasmons for short, a brief, descriptive understanding of surface polaritons is

given. The way in which surface plasmons are technically excited is then presented. There are mainly two methods available, the prism and the grating coupling, with only the prism formation being considered here in detail. Finally, the focus is put on the question how the system responds if extra layer is then added to the dielectric.

Wave-like electromagnetic modes that propagate along an interface between two media and whose amplitudes decrease exponentially normal to the surface are called surface polaritons, i.e. surface electromagnetic modes involving photons coupled to surface electric-dipole and/or magnetic-dipole excitations. A plane wave of transverse electric-dipole excitation propagating along the x-axis in an optically isotropic medium is now considered. Since the macroscopic polarization **P** is transverse and $\nabla \cdot \mathrm{P} = 0$ there are no volume polarization charges and, thus, no electric field exists. Now a non-dispersive dielectric medium is introduced with a surface normal parallel to **P**. As a result of the discontinuity in **P** a periodic surface charge density is established at the surface giving an electric field with components along x and z. Due to the fact that the surface charge density alternates in signs, the magnitude of the fields decreases exponentially in the direction normal to the surface. Furthermore, the surface charge density is the only source of the electric field and thus its z-components at equidistant points from the interface are opposite in sign. However, since the normal components of the electric displacement D at the interface in both media have to be continuous it follows that the dielectric constants $\varepsilon_1(\omega)$ and $\varepsilon_2(\omega)$ have opposite sigh. This is the basic condition for the existence of surface electric-dipole excitations. Of such an electrostatic field is coupled to 'surface photons' a so-called surface polariton is created, the total electric field of which consists of a superposition of the constituting electrostatic and electromagnetic fields. Since the

coupling photon has to provide for the surface charge density the surface polaritons are TM modes.

2.1.3 Plasmon Surface Polaritons at a Noble Metal/Dielectric Interface

The interface between two media of different frequency-dependent, but this time complex dielectric functions is examined.

$$\begin{aligned} \varepsilon_1 &= \varepsilon_1' + i\varepsilon_1'' \\ \varepsilon_2 &= \varepsilon_2' + i\varepsilon_2'' \end{aligned} \tag{2.7}$$

The link between the complex dielectric constant ε and the complex refractive index $(n + i\kappa)$ is given by

$$\begin{aligned} (n + i\kappa) &= \varepsilon' + i\varepsilon'' = \varepsilon \\ \varepsilon' &= n^2 - \kappa^2 \\ \varepsilon'' &= 2n\kappa \end{aligned} \tag{2.8}$$

The real part n is called refractive index whereas the imaginary part κ is the absorption coefficient, i.e. responsible for the attenuation of an electromagnetic wave. The magnetic permeabilities μ_1 and μ_2 are considered to be equal to 1.

As explained above, there only exist surface polaritons for transverse magnetic polarized incident plane waves. Thus, the solution to the problem will have the general form of

$$\begin{aligned} \mathrm{A}_1 &= \mathrm{A}_{01} \cdot \exp\left[i(k_{x1}x + k_{z1}z - \omega t)\right] \\ \mathrm{A}_2 &= \mathrm{A}_{02} \cdot \exp\left[i(k_{x2}x + k_{z2}z - \omega t)\right] \end{aligned} \tag{2.9}$$

with A either being the electric field **E** or the magnetic field **H**. k_{x1} and k_{x2} are the wavevectors in x-directions and k_{z1}, k_{z2} the ones along the z-axis. The numbers 1 and 2 are references to the two media involved for z > 0 and z < 0, respectively. The

continuity of the tangential components of **E** and **H** at the surface, i.e. $E_{x1} = E_{x2}$ and $H_{y1} = H_{y2}$ accounts for

$$\begin{aligned} k_{z1} H_{y1} &= \frac{\omega}{c} \varepsilon_1 E_{x1} \\ k_{z2} H_{y2} &= \frac{\omega}{c} \varepsilon_2 E_{x2} \end{aligned} \tag{2.10}$$

On the other hand, inserting equation (2.8) into Maxwell's equations (2.4) gives

$$k_{x1} = k_{x2} = k_x \tag{2.11}$$

This leads to the only nontrivial solution if

$$\frac{k_{z1}}{k_{z2}} = -\frac{\varepsilon_1}{\varepsilon_2} \tag{2.12}$$

This equation states that surface electromagnetic modes can only be excited at such interfaces where both media have dielectric constants of opposite signs, as has already been shown above. If one of the two media is a dielectric with a positive dielectric constant ε_d then the above relation can be fulfilled by a whole variety of possible elementary excitations if and only if their oscillation strength is large enough to result in a negative dielectric constant ε. For excitations like phonons or excitons the coupling to a surface electromagnetic wave leads to phonon surface polariton or exciton surface polariton modes, respectively. Another type of excitation that can couple to surface electromagnetic waves is the collective plasma oscillation of a nearly free electron gas in a metal around the charged metal ions, called plasmon surface polaritons.

In dielectrics the electrons are bound tightly to the nuclei resulting in a small, positive and real dielectric constant. In metals, however, the electrons are quasi-free and may be moved easily by an external force. The classical Drude model, which considers the electrons to be free, already derives at a highly negative, complex dielectric constant:

$$\varepsilon(\omega) = 1 - \frac{\omega_p{}^2}{\omega^2} \tag{2.13}$$

The plasma frequency ω_p usually lies in the UV range for metals. The above equation is valid for frequencies ω from 0 up to a maximum frequency $\omega_{\max}$, which is given by

$$\omega_{\max} = \frac{\omega_p}{\sqrt{1+\varepsilon_d}} \tag{2.14}$$

For metals the dielectric function, ε_m, is in general complex with a negative real part and a small positive imaginary part.

Continuing the above deduction of the very distinct wavevector of a surface plasmon, the wavevectors in the direction of the z-axis can be calculated:

$$k_{zd} = \sqrt{\varepsilon_d \left(\frac{\omega}{c}\right)^2 - k_x{}^2} \quad \text{and} \quad k_{zm} = \sqrt{\varepsilon_m \left(\frac{\omega}{c}\right)^2 - k_x{}^2} \tag{2.15}$$

Finally, with equation (2.12) this leads to the dispersion equation for surface plasmons at a metal/dielectric interface:

$$k_x = k_x' + i k_x'' = \frac{\omega}{c}\sqrt{\frac{\varepsilon_m \cdot \varepsilon_d}{\varepsilon_m + \varepsilon_d}} \tag{2.16}$$

In conclusion, the complex nature of the wavevectors in x- and z- direction leads to an exponentially decaying wave in z and an attenuated wave along the x-axis. A finite propagatin length L_x

$$L_x = \frac{1}{k_x''} \tag{2.17}$$

can be defined, which extremely influences the lateral resolution and is especially important in surface plasmon microscopy applications. For a gold/air interface with

$\varepsilon_m = -12 + i \cdot 1.3$ and $\lambda = 632.8$ nm the propagation length is in the range of L_x =10μm.

2.1.4 Excitation of Surface Plasmons

Another aspect of the dispersion relation of surface plasmons is summarized in the following equation:

$$k_{x,SP} = \frac{\omega}{c}\sqrt{\frac{\varepsilon_m \cdot \varepsilon_d}{\varepsilon_m + \varepsilon_d}} \qquad \geq \qquad \frac{\omega}{c}\sqrt{\varepsilon_d} = k_{x(\max),ph} \tag{2.18}$$

Clearly, one result of this equation is, as already stated above, that the z-component of the surface plasmon wavevector is purely imaginary. Thus, the surface plasmon is a nonradiative evanescent wave with maximum field amplitude at the interface. It

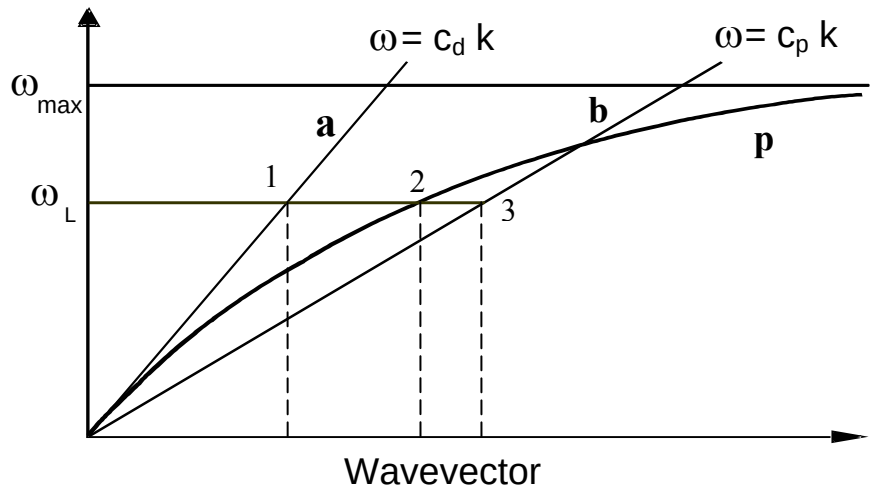

Figure 2.2: Dispersion relation of free photons in a dielectric (a) and in a coupling prism (b) with $n_p > n_d$, compared to the dispersion relation of surface plasmons at the interface between metal and dielectric. At a given laser wavelength ω_L the energy and momentum match of the photons impinging from a dielectric with the surface plasmon is not achieved whereas for the photons incident through a prism, which is increasing the pohotons momentum, it is attained.

decays exponentially into the dielectric and the metal. Another consequence is that a light beam incident from the dielectric with the maximum wavevectorv $k_{x(\max),ph}$ at the interface cannot excite a surface plasmon with the wavevector $k_{x,ph}$ since its momentum is not sufficiently large.

Figure 2.2 presents these details graphically. Although the light line of free photons (a) approaches asymptotically the dispersion curve of surface plasmons (p) there is no intersection of both curves and the x-component of the waevector of incident light is always smaller than the one for surface plasmons. Among the developed methods to increase the momentum of the light in order to couple to surface plasmons there are for example nonlinear coupling or coupling by means of a rough surface. By far the most predominant coupling techniques, however, are the prism coupling and the grating coupling, but only the prism coupling will be discussed in the following.

Prism coupling represents one way of increasing the wavevector of the incident light and hereby the x-component of the wavevector, which only couples to the surface excitation. Figure 2.2 also shows the corresponding dispersion relation if the refractive index of the prism n_p is larger than the one of the dielectric n_d. The momentum is increased, the curve more tilted and therefore at a given laser wavelength ω_l, coupling to surface plasmons (2) can be obtained. However, since at point (3) the momentum of the light beam is too large it has to be tuned to the one of the surface plasmon by varying the angle of incidence ($k_{x,ph} = \left|k_{ph}\right| \cdot \sin\theta_i$).

There exist two different configurations with which to excite surface plasmons by use of a high refractive index prism. The one that was proposed first is the so-called Otto configuration. Here, the laser beam is reflected off the base of a prism (common geometries are half-sphere, half-cylinder or 90° prisms). A gap of low refractive index, less than a few radiation wavelengths thick (for visible light < 2µm) provides for a tunnel barrier across which the evanescent radiation couples from the totally internally reflecting base of the prism to the bound surface field of the surface plasmon. Experimentally, the resonant coupling is observed by monitoring the

reflected light beam as a function of the angle of incidence. However, there is a major technical drawback to this type of configuration as one has to fulfill the need of providing a gap of approximately 200nm for efficient coupling. Even a few dust particles can act as spacers preventing a controlled assembly of the coupling system.

Fortunately, there is another method for coupling light to surface plasmons by means of a high refractive index prism – the Kretschmann configuration. In this excitation scheme the light does not couple through a dielectric layer yet, alternatively, through a thin metal layer, which is directly evaporated onto the base of the prism. At the momentum matching condition a surface plasmon is then excited at the interface between the metal and dielectrics, as depicted in figure 2.3.

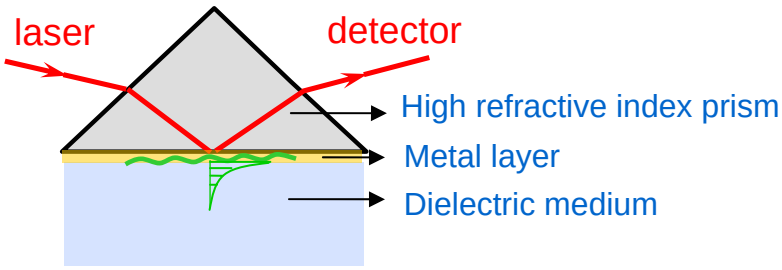

Figure 2.3: Schematic diagram of prism coupling

However, in contrast to the above derived mathematical description the surface plasmons are not restricted to two half-spaces anymore. Quantitatively, one has to take the finite thickness of the metal layer into account, which allows in particular that some of the surface plasmon light is coupled out through the metal and the prism. This new, additional rediative-loss channel, however, can be considered as a minor perturbation to the surface plasmon electromagnetic wave. In any case, it is clear that there exists an optimum thickness of the metal: taken that the metal film is too thin damping of the surface plasmon wave will occur due to the radiative loss channel

back through the metal film and the prism. If the metal layer is too thick the tunnel barrier is too large and only little light will couple to surface plasmons at the metal/dielectric interface. For both, gold and silver, the optimum thickness for a laser wavelength of $\lambda = 632.8$ nm lies between 45nm and 50nm, which can be easily controlled by evaporation.

2.1.5. Surface Plasmon Spectroscopy

As high refractive prisms are used for the excitation of surface plasmons in the examples of figure 2.3, the momentum of the incident light beam in the plane of the

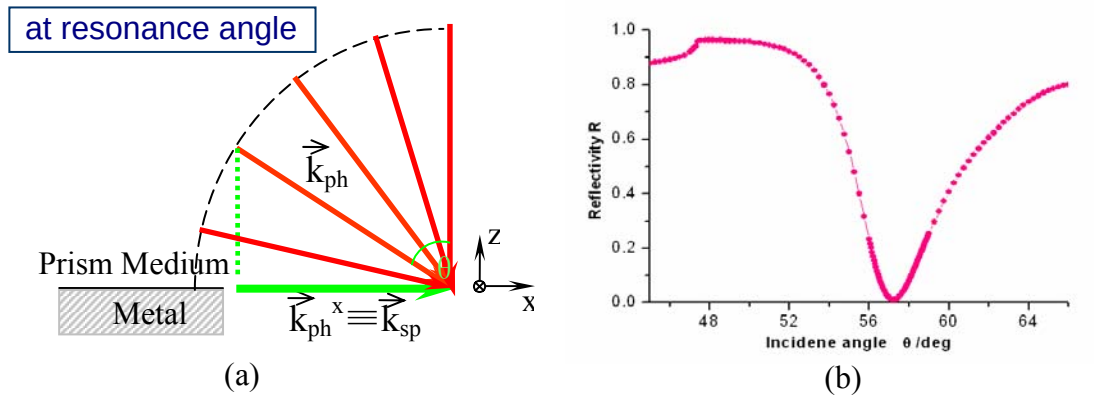

Figure 2.4: (a): The momentum of the incident light beam in the plane of the interface exceeds the one needed for the excitation. Thus, it is possible to tune the system into resonance by simply changing the angle of incidence; (b): A typical angular scan of Surface Plasmon Spectroscopy.

interface exceeds the one needed for the excitation. Thus, it is possible to tune the system into resonance by simply changing the angle of incidence, as $k_x = k_0 \cdot \sin\theta_i$. This situation is schematically shown in figure 2.4 (a) and (b).

At low angle, the reflected intensity increases, as described by the Fresnel formulas. Then, from a certain angle, the angle of total reflection θ_c, onwards it reaches a plateau. Note, firstly, that the reflectivity before θ_c is rather high, which is due to the evaporated metal film that acts as a mirror reflecting most of the incident light. Secondly, the maximum reflected intensity never reaches unity since the photon

energy is partly dissipated in the metal layer. Lastly, the position of the critical angle only depends on the substrate and superstrate, i.e. prism and water, and is not influenced by any of the intermediate layers. If the projection of $\mathbf{k}_i$ to the interface matches $k_{x,SP}$ resonance occurs and a surface plasmon is excited. This condition is given at the intersection 2 of figure 2.3. Once the system is in resonance surface electromagnetic waves are excited, which can be observed as a dip in the reflected intensity. The minimum is denoted by θ_0 (angle of incidence inside the prism θ_0') and is given by

$$\theta_0' = a\sin\left(\sqrt{\frac{\varepsilon_m \cdot \varepsilon_d}{(\varepsilon_m + \varepsilon_d)\cdot \varepsilon_p}}\right) \tag{2.19}$$

with ε_p being the dielectric constant of the prism. As mentioned above, for real metals there is resistive scattering and hence damping of the oscillations created by the incident electromagnetic field. (If not the surface plasmon resonance would be infinitely sharp and have an infinite propagation length.) The imaginary part of the dielectric constant of the metal causes the damping and the dispersion relation for surface plasmons can be rewritten as:

$$k_x = k_x' + ik_x'' = \frac{\omega}{c}\sqrt{\frac{(\varepsilon_m' + i\varepsilon_m'')\cdot\varepsilon_d}{(\varepsilon_m' + i\varepsilon_m'') + \varepsilon_d}} \approx \frac{\omega}{c}\sqrt{\varepsilon_d}\left(1 - \frac{\varepsilon_d}{2\varepsilon_m'}\right) + i\cdot\frac{1}{2}\frac{\omega}{c}\frac{\varepsilon_m''(\varepsilon_d)^{3/2}}{(\varepsilon_m')^2} \tag{2.20}$$

Thus, the shift of surface plasmon is inversely proportional to ε_m' whereas the width, which is related to k_m'', depends on ε_m'' and is inversely proportional to $(\varepsilon_m')^2$. While at first sight it might therefore be beneficial to have a small imaginary part of the metal dielectric constant the real part is of even higher significance. Clearly, silver with the higher absolute value of ε_m' and the smaller imaginary part can be identified having a much sharper resonance.

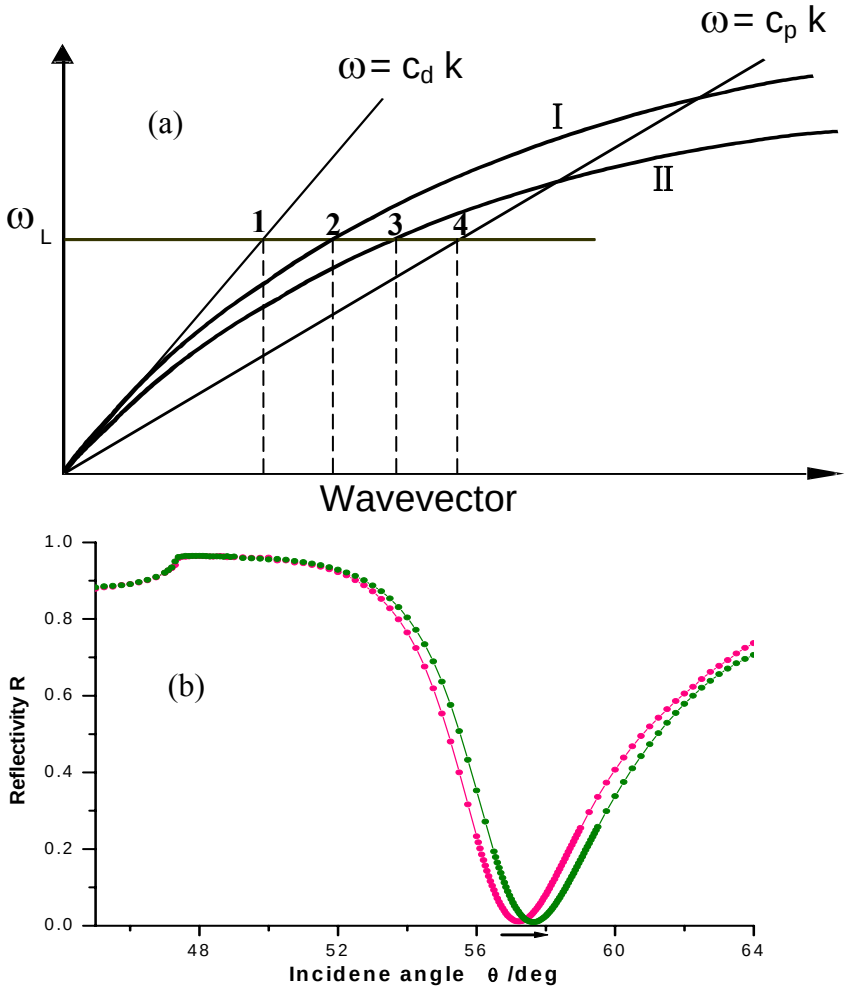

Figure 2.5: (a): Dispersion relation of surface plasmons at the interface between metal and dielectric before (Ⅰ) and after (Ⅱ) the absorption of an additional layer, compared to the dispersion relation of free photons in a coupling prism; (b) Comparison of full angular scans before and after the absorption of an additional layer. Note the moving of the maximum resonance angle.

The advantage of surface plasmon spectroscopy lies in its sensitivity to surface processes due to its evanescent field. This means, on the one hand, that a change of the dielectric, i.e. ε_d in equation (2.19), leads to either a drop or an increase of the wavevector of the surface plasmon resonance, depending on the sign of the change. For example, the resonance angles θ_0 for air and water can be found at low and high angles, respectively. On the other hand, the addition of a thin layer ($d << 2\pi / k_{zd}$) of a second dielectric to the already existing triggers a changed surface plasmon response and the corresponding shift of the dispersion curve is equivalent to a change

of the overall refractive index integrated over the evanescent field. The net effect is a slight shift of the surface palsmon dispersion curve as can be seen in figure 2.5 (a) for an additional layer with higher refractive index than the one of the reference dielectric medium. At the same energy $\hbar\omega$ of incident light the dispersion curve of the surface plasmon intersects with the light line at a higher wavevector (point 4 in fig 2.5 (b)). In terms of the reflectivity as a function of the angle of incidence the minimum is therefore shifted to higher angles.

When adding a layer to the existing system two parameters are of interest, the refractive index and the thickness of the film. In order to separate these two parameters at least two distinct features that are correlated to the addition are needed. Yet, the surface plasmon resonance only provides one. Consequently, only a set of parameters (n, d) can be derived from such reflectivity curve, provided both parameters are unknown. If one of them is known the other one can be obtained from fits to the curves. Several methods resolve the ambiguity of this problem. Firstly, resonance curves can be taken at different laser wavelengths. This method, however, dose not resolve the ambiguity of the unknown dispersion behavior of the refractive index of the coating. Secondly, the contrast of the experiment can be varied, i.e. the surface plasmon curves are measured in at least two solvents with different refractive indices. The minimum shift does not depend on the absolute value of n but rather on the contrast, i.e. the refractive index difference between the layer and the surrounding medium. In both of the presented methods a set of at least two different curves of n vs. d is obtained, the intersection of which determines the correct refractive index and thickness of the additional layer. Finally, if the aim of the study and the chemicals allow for the preparation of thick films, waveguide modes can be excited. If the film

is sufficiently thick and an adequate number of modes is available, *n* and *d* can be evaluated separately and even the indicatrix may be obtained.

2.2 Fluorescence

Analytical methods incorporating fluorescence based detection are widely used in chemical as well as biochemical research due to the extraordinary sensitivity and the favorable time scale on which fluorescence occurs. A number of molecular processes can be observed by monitoring their influence on a fluorescent probe during the fluorescence lifetime, which is typically in the range of 10ns. The impact of this technology in biochemical research has been shown previously. Immunoassays relying on fluorescence detection (fluoroimmunoassays, FIA) may replace established radioimmunoassay if such limitations like relatively high fuorescence background signals can be reduced [16-18].

Several photophysical parameters of fluorescent probes have been exploited to monitor analyte binding events. These include fluorescence polarization [19], fluorescence quenching [20, 21], fluorescence enhancement and resonant energy transfer (RET) [22, 23]. Combining one of these fluorescence schemes with other optical or electrical detection methods of interest can lead to an improvement in the sensitivity and detection limit of these methods. Since fluorescence detection has been utilized extensively in this work, the underlying principles shall be explained in the following.

Fluorescence is a well characterized phenomenon which describes the emission of photons from molecules that undergo a transition from an electronically excited to the ground state [24]. Fluorophores often exhibit strongly delocalized electrons in conjugated double bonds or aromatic systems. The molecular processes during

absorption and emission of photons are illustrated by the schematic Jablonsky energy level diagram shown in Figure 2.6.

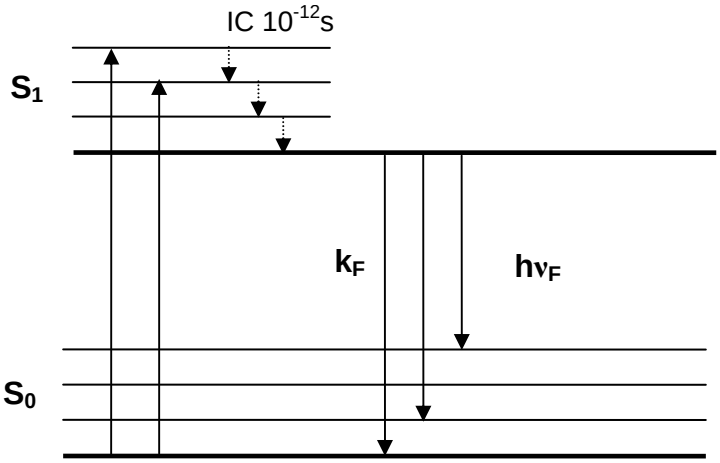

Figure 2.6: Jablonsky diagram illustrating the electronic and vibrational states of a fluorophore and processes during photon absorption and fluorescence emission.

A fluorophore may exist in several electronic states, two of which are depicted here (S_0 and S_1). These levels are described by the spin multiplicity of the state, so that e.g. singlet and triplet states can be found, depending on how the orbits of the molecule are populated and how the spins of the electrons are paired. Triplet states are not involved in the fluorescence mechanism itself, so that we concentrate on the singlet levels only. At each of these electronic levels the fluorophore can exist in a number of vibrational levels, which are populated according to the Boltzmann distribution law [25]. Hence, at room temperature and a given energy spacing of the levels most of the molecules will be present in the lowest vibrational level of S_0. Following light absorption, the fluorophore is excited to some higher vibrational levels of S_1 or S_2 (not shown) in the time scale of 10^{-15}s. The absorption spectrum therefore reveals information about the electronically excited states of the molecule. Generally, the system relaxes into the lowest vibrational level of the S_1 state by internal conversion (IC) occurring in about 10^{-12} s. Since fluorescence lifetimes are typically around 10^{-8} s

relaxation to the thermally equilibrated ground state of S_1 is complete prior to emission of photons and consequently fluorescence starts from the lowest vibrational level in S_1 (Kasha's rule) [26]. From there the molecule can decay to different vibrational levels of the state S_0 by emitting light (with a rate constant k_F). This leads to the fine structure of the emission spectrum by which we can gain information about the electronic ground state S_0. The transition between two states of the same spin multiplicity is a quantum mechanically allowed process and therefore reveals high emissive rates of typically near $10^8\ s^{-1}$.

Comparing absorption and emission spectra one observes the so called Stokes' shift of the fluorescence emission to lower wavelength (red shift) relative to the absorption. This shift can be explained by energy losses between the two processes due to the rapid internal conversion in the excited states (S_1, S_2) and the subsequent decay of the fluorophore to higher vibrational levels of S_0. This shift is fundamental to the sensitivity of fluorescence techniques, because it allows the emitted photons to be isolated from excitation photons detected against a low background. In contrast absorption spectroscopy requires the measurement of transmitted light relative to high incident light levels of the same wavelength. Generally, the fluorescence emission spectrum appears to be a mirror image of the absorption spectra, because of the same transition that are involved in both processes and the similarities among the vibrational levels of S_0 and S_1. Often deviations to this mirror rule can occur due to e.g. excited state reactions and geometric differences between electronic ground and excited states.

A fluorescence emission spectrum is recorded by holding the excitation wavelength constant and detecting the fluorescence intensity over a range of emission wavelengths. In contrast to this, an excitation spectrum is recorded by holding the

emission wavelength constant and scanning over a range of excitation wavelength. With a few exceptions the excitation spectrum of a fluorescent species in dilute solutions is identical to the absorption spectrum. Under the same conditions, the fluorescence emission spectrum is independent of the excitation wavelength.

3. Experimental Methods

A major part of this work is based on the characterization of surface processes like adsorption and desorption of analytes onto dielectric thin films of known architecture. Surface plasmon spectroscopy (SPS), as a prominent optical method, permits the detection of such processes on metal substrates and is therefore described in detail. Furthermore the experimental construction of simultaneous fluorescence detection in Surface Plasmon Fluorescence Spectroscopy (SPFS) and Surface Plasmon Fluorescence Microscopy (SPFM) will be discussed. Finally the combination of both methods with microscopy and the resulting possibility to analyse laterally structured samples will be discussed.

3.1 Surface Plasmon Spectroscopy

Since the theoretical background of surface plasmons was already discussed in chapter 2, the measurement modes of SPS are described in the following. The experimental setup is illustrated in figure 3.1.

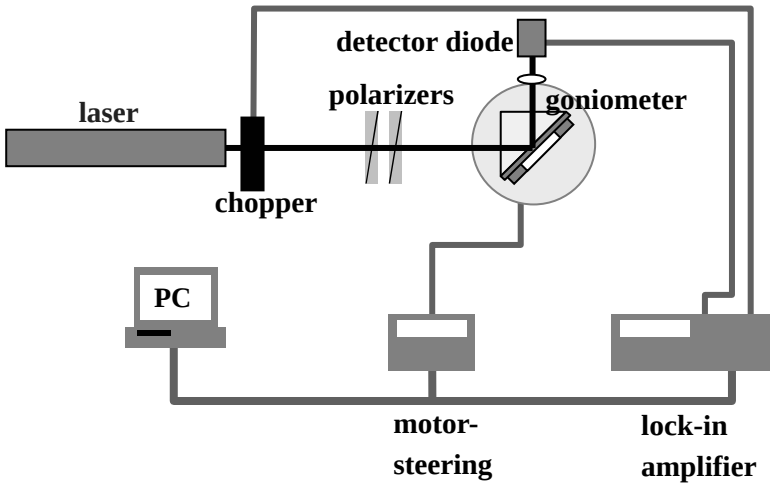

Fig.3.1: Schematic diagram of Surface Plasmon Spectroscopy (SPS) setup

In the following, some experimental issues of surface plasmon spectroscopy are presented beginning with the different types of measurement modes. Starting from the basic angular measurement as already discussed above the time dependent modus is sketched with which adsorption kinetics, molecular switching behavior or other time dependent surface processes can be studied. The second part is concerned with the experimental setup of the normal SPS version and its various extensions.

As explained, a resonance spectrum (also referred to as scan curve) is obtained by reflecting a polarized laser beam off the base plane of a prism and plotting the normalized reflected intensity versus the incidence angle. The range of the angles measured is important, since the resulting scan should cover the total reflection edge and most of the resonance minimum. The obtained scan curve can then be fitted according to Fresnel's formula in order to calculate the thickness of the metallic and dielectric layers. The calculations based on the transfer matrix algorithm are carried out with the computer software Winspall 2.0, which was developed in our group. Parameters that are included in the fitting procedure are the measured reflectivity, the incidence angle, thickness and dielectric constants of the layers as well as the used laser wavelength and the geometry of the coupling prism. By iterative optimization of the parameters the simulated reflectivity curve is fitted to the measured scan curve and the optical constants of the involved layers are determined.

Since the thickness and dielectric constant of the layers cannot be determined independently, one of the parameters has to be measured by use of other techniques.

However, if the refractive index of the prism is known, the refractive index of a used solvent can be easily calculated by determining the critical angel. The angular position of the total reflection edge is only dependent on the optical constants of both outer media.

The adsorption of an additional layer (e.g. a self assembled monolayer of thiols on gold) changes the optical properties of the dielectric next to the metal and results in a shift of the resonance minimum as schematically depicted in figure 3.2. This shift can be theoretically considered by introducing an additional layer into the Fresnel simulations while the parameters of the other layers are held constant. Such a comparison between the simulated parameters before and after the adsorption process allows for the determination of the thickness or refractive index of a layer adsorbed to the metal.

Not only static measurements of film-thickness and refractive index can be obtained but also the online monitoring of processes near the surface is possible and kinetics of surface reactions can be recorded. For this purpose the incidence angle is fixed at a

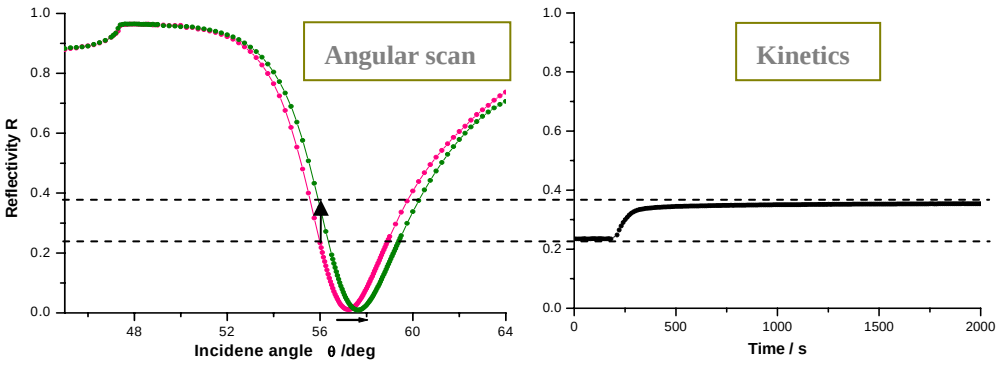

Figure 3.2: Angular scan curves and associated kinetic measurement. Note that the reflectivity is increased if the incidence angle is fixed and the resonance curve is shifted.

position for which the measured scan curve exhibits a linear slope (e.g. at 30% reflectivity) and the detected reflectivity is recorded with time. The reflectivity at this fixed incidence angle is increased if the resonance is shifted towards higher angles and the detected shift represents a linear time dependence of the optical properties of the investigated system. Here it is assumed that the dependence of the resonance minimum shift on optical changes is linear, too. In addition, it is assumed that the shape of the scan curve in the considered region is not changed upon adsorption of the additional layer. Otherwise the linear response of the kinetic curve would be lost.

3.2 Surface Plsmon Fluorescence Spectroscopy (SPFS)

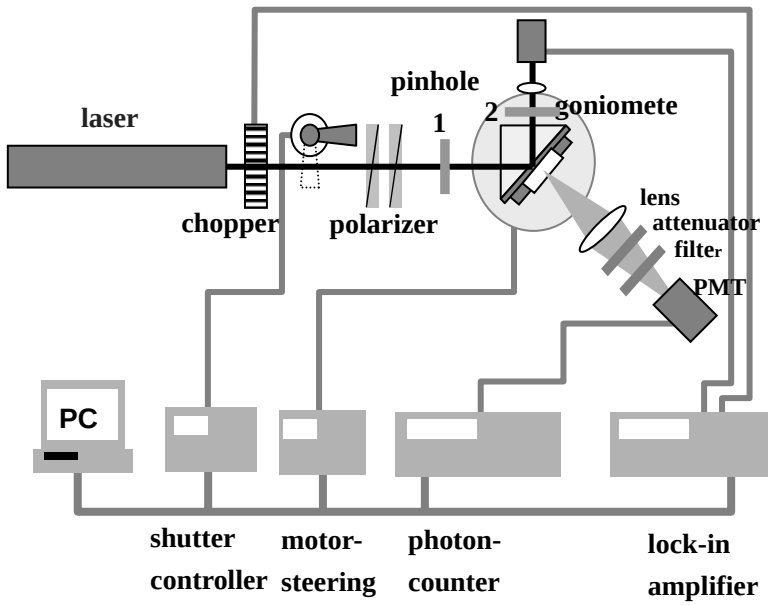

Figure 3.3: Surface Plasmon Fluorescence Spectroscopy (SPFS) set-up.

It will be shown that the fluorescent molecules near surfaces can be excited by the evanescent field of surface plasmons. In the following the experimental set-up and the measurement principle will be discussed and the analysis and interpretation of the data will be explained.

The setup is a common surface plasmon spectrometer which was modified with fluorescence detection units. As schematically depicted in figure 3.3, a HeNe laser (Uniphase, 5 mW, λ = 632.8 nm or 5mW, λ = 543 nm), the excitation beam passes two polarizers, by which the intensity of the incident light and its TM polarization can be adjusted. Using a beam splitter and two programmable shutters the incident wavelength can be easily changed by blocking one of the laser beams and passing the other laser onto the sample.

The incident laser is reflected off the base plane of the coupling prism (Schott, 90°, $LaSFN_9$) and the reflected intensity is focused by a lens (L2, f=50mm, Ovis) for detection by a photodiode. In order to allow for noise reduced and daylight independent measurements of the reflected intensity, the photodiode is connected to a lockin-amplifier. This unit filters out all frequencies that are not modulated by the operation frequency of the attached chopper. If working in a lab environment multiple frequencies of 50 Hz should be avoided, since this is the frequency of electric ceiling lamps for example.

The sample is mounted onto a 2 phase goniometer (Huber) which can be rotated in $\Delta\theta$ = 0.001deg steps by the use of the connected personal computer. According to the reflection law the angular position of the optical arm holding the detection unit (detector motor) is adjusted during the measurements. The sample is mounted onto a table which can move and tilt to allow for the optimal adjustment of the setup. This adjustment is described in detail in the next section.

In order to detect the fluorescence emission of the sample a collecting lens (f = 50mm, Ovis) focuses the emitted light through an interference filter into a photomultiplier tube (PM1, Hamamatsu), which is attached to the backside of the sample. The photomultiplier is connected to a counter (HP) via a photomultiplier protection unit and a programmable switch box. Thus, the signal of PMT unit can be recorded by the online personal computer. The protection unit closes the implemented shutter in front of each photomultiplier if the irradiation exceeds a predefined level in order to avoid damage of the sensitive fluorescence detection equipment.

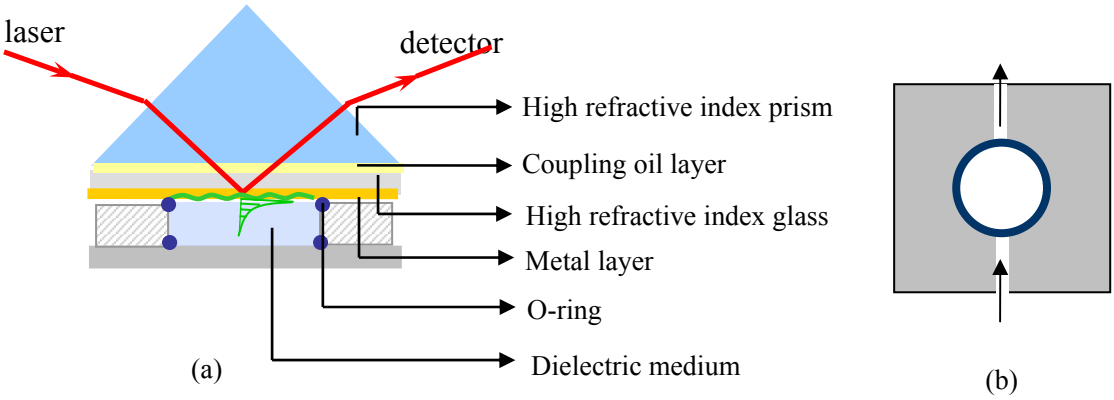

Figure 3.4: (a) Mounting of the prism, sample and flow cell.
(b) The lattice of flow cell.

Preparation of the Flow Cell

As schematically shown in figure 3.4 the flow cell made of quartz glass (Herasil, Schott) is placed onto a low-fluorescent quartz glass slide (Herasil, Schott) and sealed by O-rings made of Viton. The glass waver is placed on top of the flow cell, while the evaporated metal film points towards the cell. Finally a high refractive index prism ($LaSFN_9$) is mounted on top of the glass sample. To allow for optional coupling of incident light into plasmon modes of the metal, a thin film of refractive index

matching oil is added in between both glass units. This fluid should have a similar refractive index as prism and glass in order to allow for unperturbed coupling. The higher the refractive index of this fluid the higher the vapor pressure and the easier the fluid is evaporated at room temperature. For practical reasons a less volatile index matching liquid is frequently used with the drawback of a lower refractive index and thus non optimal match. The flow cell is equipped with an inlet and outlet and can hold volumes up to ca. 90ul. For the injection of analyte samples one-way plastic syringes are used, but to rinse the cell with pure buffer and to rinse the sample after adsorption processes a peristaltic pump is used.

In order to align the measurement system two apertures are mounted into the incident and reflected beam. Without having the sample mounted in the setup the detector arm is moved to 180° to align the height of pinhole 2 and to adjust the position of the photodiode. The incident laser should pass through both apertures and the position of the laser spot on aperture 2 should not change upon movement of the pinhole along the detector arm. Otherwise the height of pinhole 2, the orientation of the photodiode and the angular position of the detector arm have to be optimized.

The sample is mounted into the setup and the sample motor moved to 45° while the detector arm moves to 90° according to the reflection law. At this angle, a part of the incident beam should be reflected and the prism-air interface. The back reflex should be directed back into pinhole 1, while the reflection on the prism-gold interface should pass pinhole 2. Sometimes two laser beams are reflected back to aperture1.

Then the light beam that does not change the intensity upon variation of the incident angle is the one that should be used for the 45° adjustment. The additional beam was caused by multiple reflections inside the prism and shows a reflectivity minimum due to reflections onto the prism-metal interface. Both tilting tables have to be used in order to align the height of the reflected laser beams on aperture 2 and 1, respectively.

The beam point of the incident laser light on the gold sample and the reflected light on aperture 2 should be fixed, if sample and detector motor are moved by θ and 2θ, respectively. In case of such a movement of the laser spot during the scan, the prism has to be adjusted in the z-direction. Thus the axis of rotation in the prism according to the incident laser beam has to be aligned. Once the beam point is fixed, the prism is moved in x direction in order to hit the centre of the sample. Both apertures are finally opened before the first measurement is started.

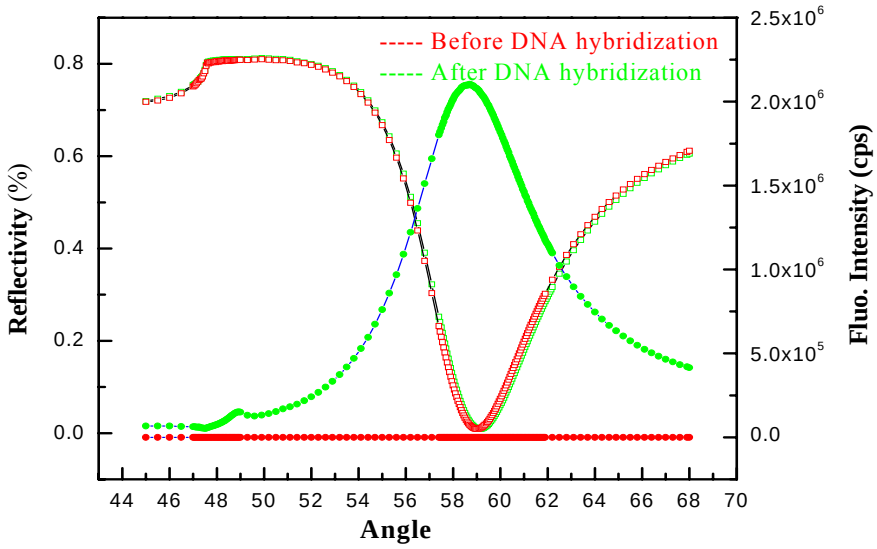

Figure 3.5: Typical SPFS curves before and after adsorption of fluorescence DNA target oligonucleotide.

In case of simultaneous fluorescence measurements, the lens at the back of the sample substrate in Figure 3.4 is adjusted to focus the emitted fluorescence light onto the photomultiplier unit.

The simultaneous detection of the fluorescence by the attached photomultipliers during a scan is controlled by a software routine that moves both goniometers in predefined steps, records the actual fluorescence intensity that was measured by the counter and finally collects the reflectivity from the lockin-amplifier. Hence, in the resulting fluorescence scan curve (counter-scan) the measured intensities and reflectivity can be assigned to the same incidence angles. Typical curves before and after adsorption of fluorescence DNA target oligonucleotide are shown in Figure 3.5. Due to the low molecular weight of the used analyte no change of the resonance minimum and of the reflectivity can be seen.

Before the adsorption of the fluorophores a background signal of about 5000cps is detected for all angles larger than the critical angel, caused by the intrinsic fluorescence of the used prism. The slight increase of fluorescence before the total reflection edge can be explained by incident light that passed the interference filter IF1 due to its half-width. Additionally, scattered light may influence the measurement signal. For angles larger than the critical angle the incident laser light is reflected completely and does not influence the measured intensities. However, the excitation of the adsorbed fluorophores in the plasmon field leads to a strong fluorescence intensity in the scan. The angular dependence of this intensity follows the already

described electromagnetic field intensity. It can be found to be maximal next to the resonance minimum, where the excitation of surface waves is the strongest.

Starting from the background of ca. 5000 cps the counter-kinetics reflects the increase of the fluorescence emission at the fixed angle of 59°, where the linear part of the reflectivity can be found. At this incident angle no change in the reflectivity was observed. Therefore the time dependent fluorescence measurement reflects changes in the signal under constant excitation conditions. Note, that in case of large shifts of the underlying counter scan curves a deviation has to be considered. The signal needs to be compensated, since the fluorescence would be altered due to changes in the relative position on the fluorescence peak. We assume that no inner filter effects or photo bleaching influence the observed fluorescence signal. However, the measured intensity is not directly convertible into the number of adsorbed fluorophores. This conversion requires the possibility of calibrating the measured fluorescence to an angular resonance shift and hence to a measurable layer thickness. In cases where SPS alone is not sensitive enough to detect the adsorption of low molecular fluorescent dyes, a theoretical calibration approach is rather difficult.

However, the difference between the observed fluorescence increase during the adsorption of the labeled molecules and the virtually unchanged reflectivity demonstrates the sensitivity enhancement of surface plasmon spectroscopy (SPS) by the additional fluorescence detection in SPFS.

The experiments carried out in this work may vary in measuring type and sequence.

In general the following measurement sequence was used frequently to monitor adsorption and desorption processes on the surface.

1. Scan curve: To determine the thickness of the used metal film and to obtain a measure for the fluorescence background of the sample a counter scan is recorded. Eventually, the cell was filled with the pure buffer, which was used to dissolve the analyte of interest.
2. Kinetic run: The analyte to be tested is dissolved and injected into the flow cell after the observed baseline was found to be stable. After the adsorption process is finished, the sample is rinsed with pure buffer, so as to remove bulk analytes and unspecifically bound molecules from the sample surface.
3. Scan curve: In comparison with the reference scan the change in thickness, refractive index and fluorescence signal is determined as explained before.

This sequence has to be carried out for every single layer on the sample so that each additional layer can be characterized separately.

3.3 Sample Preparation Techniques

3.3.1 Thermal Evaporation of Metal Layers

The gold and silver metal needed for surface plasmon experiments are thermally evaporated onto the sample in commercially available evaporation chambers. For prism experiments, layer thicknesses between 45 and 50nm are evaporated, depending on the metal (purity 99.99%). The evaporation is started at a vacuum pressure of around 1×10^{-4} Pa and the evaporation rate is set to 0.1 nm/s.

3.3.2 Cleaning procedure

Residual organic contaminations on the sample can be removed by exposure to piranha solution (H_2O_2 and HNO_3 in a ratio 1:2). Old metal films are easily removed by a iodine solution (40g iodine, 40g potassium iodide and 100ml MilliQ water).Once all organic or metal coatings have been removed the samples are further cleaned by the following procedure:

- 15× rinsing in purified water (MilliQ, *Millipore*)
- 15 minutes cleaning in an ultrasonic bath with a solution of 2% detergent (Hellmanex, *Hellma*) in MilliQ water
- Again 15 minutes cleaning in an ultrasonic bath with a solution of 2% detergent (Hellmanex, *Hellma*) in MilliQ water
- 20× rinsing in purified water
- 5 minutes cleaning in an ultrasonic bath with ethanol
- Drying of the glass samples in a flow of nitrogen gas

3.3.3 Self-Assembled Monolayers on Metals

Self-assembled monolayers (SAMs) are molecular assemblies that are formed spontaneously if an appropriate substrate is immersed into a solution of an active surfactant in a solvent. The popularity of these layers stems from the fact that well-defined and closely packed assemblies can very easily be prepared at ambient laboratory conditions and that the strong co-ordination of the head group of the surfactant to the metal yields a layer that is sufficiently stable to desorption. Moreover,

the physical-chemical properties can be tailored by the choice of the end functional group as for example –COOH, -OH, -CH_3, or –biotin and by varying the length of the alkyl chain. From a thermodynamic point of view several parameters promote the self-assembly process on the surface: Chemisorption of the head-group of the surfactant leads to a strong attractive and exothermic interaction with the surface. Consequently, all available binding sites at the surface are occupied. Additionally, attractive van der Waals interactions between the alkyl chains of the molecules can stabilize the molecular assembly.

Prominent examples of self-assembled monolayers are alkanethiol in gold, silver and copper, several sulfides on gold, alcohols on platinum and carboxylic acids on aluminum oxide. In this work only thiols are used for the adsorption onto gold and silver surfaces. The sulphur groups exothermally bind to the surface whereas the alkyl chains are oriented uniformly with an angle of 30° to the surface normal if an appropriate alkyl chain length, head group and dilution have been chosen.

If not mentioned otherwise, a 0.1 mM solution of a 9:1 mixture of biotinylated thiols and OH-terminated thiols was prepared in ethanol and the gold or silver/gold samples were immersed into this solution for 30 min. The latter served as lateral spacers for the biotin moieties to allow for optimal streptavidin binding. The samples were rinsed by ethanol and then by PBS buffer (0.01 M phosphatebuffer: 0.0027 M KCl, 150 mM NaCl, pH 7.4, Sigma) prior to further self assembly steps. The exact composition of the thiol-streptavidin architecture is discussed in detail in the results section. The self

assembly kinetics of the individual steps was monitored by SPS as described before.

3.3.4 Spincoating

The well-established technique of spin-casting is used to prepare thin polymer films in the thickness range of a few nanometers to micrometers. The material is dissolved in an appropriate solvent with, if possible, a rather high boiling point. The sample is then covered completely with this viscous solution and the spin-coater is set to rotation speeds between 1000rpm and 8000rpm for 60s. During the rotation the solution is distributed homogeneously over the surface whereas most of the solvent evaporates. The relation between viscosity of the solution and rotation speed sets the final thickness of the film. Subsequent to every spin-coating process the samples are annealed under vacuum for at least 10 hours to let all the residual solvent evaporate. For that, the temperature is set to a value well above the boiling point of the solvent but below the melting point of the respective polymer. Before letting it cool off at a very slow rate to avoid residual stress in the spin-cast layer, the temperature is raised for some minutes above the glass transition point of the film in order to remove any anisotropy in the film.

4. Results

In recent years much effort has been directed towards the development of optical biosensors. While direct sensors are capable of monitoring the presence of the analyte without use of labeling agents the group of indirect sensors exploit the signal enhancement caused by bound marker molecules. Surface Plasmon Spectroscopy (SPS) as a direct detection method is known to lack sensitivity for the detection of low mass analytes. In order to enhance the sensitivity and to improve the detection limit the technique was combined with fluorescence methods in Surface Plasmon Fluorescence Spectroscopy (SPFS) as described recently. The theory of plasmon excitation and the experimental realization of SPFS were already introduced in the experiment part.

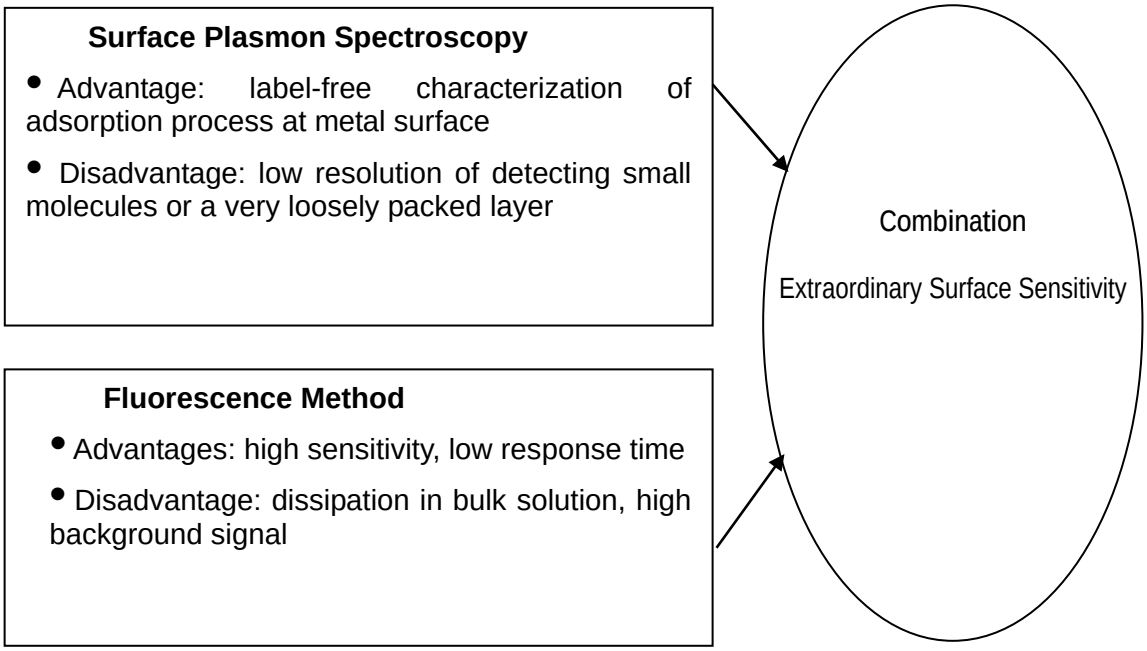

Figure 4.1: The combination of SPS with fluorescence method can obtain extraordinary surface sensitivity

From the view point of biomolecular architectures metal surfaces are very important in respect to the immobilization of molecules and for the self assembly and self

organization of lipids, proteins and nucleic acids. For instance, the detection of DNA on surfaces is based on the preparation of immobilized multilayers on thiol tethered gold surfaces. Furthermore, the presence of a metal surface is essential for the SPFS technique since fluorescent dyes in the proximity to the surface can be excited by the evanescent surface plasmon field. The detection of biomolecular binding events is entirely based on the interaction of the fluorophores with the surface fields.

In the following, all the experiments were performed using the prism coupling setup as introduced in the part of experiment method.

4.1 Theoretical Considerations

As outlined in part 2, the electromagnetic field at the surface upon the excitation of plasmons in a metal film depends on factors like the optical properties of the layer system, the metal and the incidence angle of the exciting laser beam. In the case of total internal reflection (TIR) conditions (for instance a plain glass prism in contact with a dielectric) only a moderate field enhancement by a factor of 4 is obtained at the critical angle due to constructive interference between the incoming and reflected electromagnetic field. The presence of a thin noble metal film on the prism changes the situation significantly. The evanescent field at the glass-dielectric interface can be used to resonantly excite surface plasmons in the metal and thus electrical field of incoming light is enhanced close to the resonance minimum. In the case of gold a maximum enhancement factor of about 20 is found while less damping of electromagnetic waves in silver leads to a factor of as high as 80.

In the past, it has been shown that fluorophores close to the metal surface experience this enhanced evanescent plasmon field and consequently will be excited resonantly. Such excitation of fluorescence via surface plasmons has been observed for planar

systems using prism coupling as well as for grating coupling. Only a few studies are known which use the surface sensitive enhancement for sensing purposes. As discussed in part 2, the evanescent field decays exponentially into the dielectric layer adjacent to the metal film. The penetration depth into the dielectric, at which the surface field intensity drops down to 1/e of the interface value, is in the order of the used wavelength. Thus, surface sensitive fluorescence measurements are possible, since only dyes in the proximity to the metal film contribute significantly to a measurable signal. Fluorophores further away from the metal surface cannot be excited due to a negligible evanescent field.

Compared to conventional TIRF the excitation of fluorescence via plasmons is favorable due to the following considerations: it is desirable to maximize the surface field intensity to enhance fluorescence emission while simultaneously reducing the field penetration depth in order to avoid excitation of bulk dyes in solution. For TIRF a compromise has to be made, since both penetration depth and enhancement factor reach a maximum at the critical angle. No such compromise is necessary for SPR enhancement. Furthermore, tests with fluorescently labeled antibodies proved that fluoroimmunoassays based on SPR excitation are at least 5 times more sensitive than the TIR technique.

Summarizing, SPFS is a valuable tool that allows for a surface sensitive investigation of fluorophores. Due to various advantages over common TIRF detection the SPFS technique is the method of choice.

4.2 Energy transitions for fluorescence near metal surfaces

Consider a fluorophore that is excited by either direct illumination or by an evanescent surface plasmon field in front of a planar metallic surface. Since the metal

film serves as a mirror the reflected field interferes with the emitting dipole. If the reflected field is in phase with the dipole oscillations, it will be excited by the reflected electromagnetic wave. The dipole will be driven harder and consequently the emission will be enhanced. If the reflected field is out of phase, the emission will be hindered. Thus, the dipole can be considered as a forced, damped, dipole oscillator: it is forced in the way that the field reflected by the boundary provides a driving term for the oscillation of the dipole and it is damped because the oscillator radiates power. With increasing distance between the dipole and the metal surface the phase difference between incident and reflected light alters, which results in an oscillating emission rate of the dipole. Furthermore, with increasing distance of the dye to the metal, the strength of the oscillation will decrease. The radiation field of the dipole at the surface weakens with increasing distance to the surface and thus the strength of the reflected field will also decrease. In addition to these features a strong quenching of the fluorescence light was found for small emitter-surface separations. This phenomenon could not be explained by simple interference and was attributed to direct coupling between the dipole fields and the surface plasmon modes.

The coupling between the excited (donor) states in the dye molecule and the broad band acceptor states in the metal give rise to a distance dependence of the fluorescence emission. The distance dependence of the scaled fluorescence intensity can be described by equation (4.1). [27]

$$\frac{I_d}{I_\infty} = \left[1 + \left(\frac{d_0}{d} \right)^4 \right]^{-1} \tag{4.1}$$

Here, I_∞ denotes the fluorescence intensity at infinite separation distance, i.e. in the absence of any metallic surface, I_d is the observed fluorescence intensity with the

chromophore layer being separated at a distance d from the surface. d_0 is called the Förster radium and gives the distance at which the fluorescence intensity decreased by a factor of 2 compared to the unquenched state.

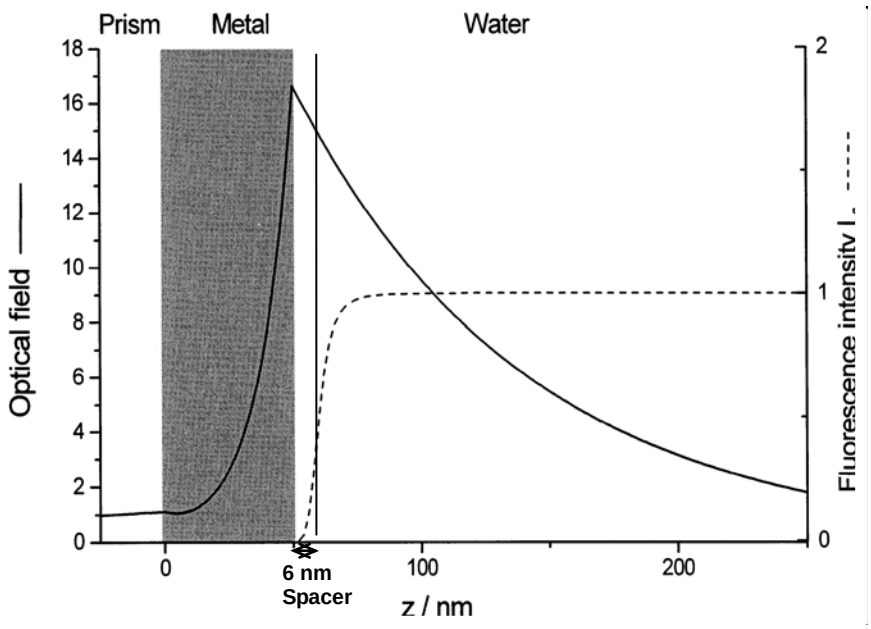

Figure 4.2: Schematic comparison of the distance dependence of the optical field of PSP mode, resonantly excited at a prism/50 nm Au/water interface (full curve), and the Förster energy transfer mechanism, expressed as the relative fluorescence intensity (dashed curve) placed at a certain distance above the metal/water interface

Distance dependence of energy-transfer mechanisms (Figure 4.2) requires a spacer layer between chromophores and metal surface to reduce quenching and to optimize fluorescence detection. By carefully designing the supramolecular interfacial layers that provide the binding sites for a biorecognition process of a fluorescently labeled analyte, one can gain high detection sensitivity by exploiting the enhanced optical field of a resonantly excited surface plasmon mode as the 'light source' without paying for fluorescence emission loss caused by quenching mechanism to the metal.

In this study, to optimize fluorescence emission without sacrificing the high enhancement of optical field of the resonantly excited surface plasmon mode, a metal-dye distance of about 6 nm is designed by carefully building up the interfacial layers.

4.3 SPFS recording of the adsorption of Organic dye- labeled streptavidin to the surface immobilized biotin-thiol

The first example that is discussed concerns the binding of streptavidin to biotin-functionalized thiol monolayer at the interface, with each streptavidin molecule being labeled with organic fluorophores. The layer architecture at the interface is schematically displayed in Figure 4.3.

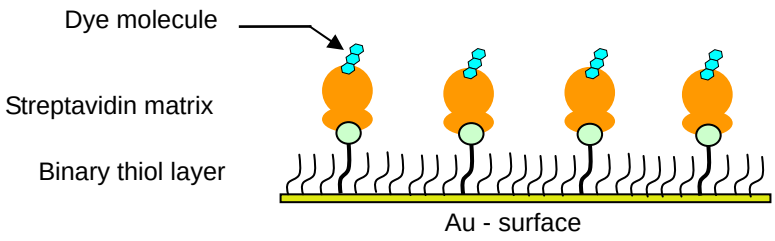

Figure 4.3: Architecture of dye-labeled streptavidin monolayer.

First, the gold substrate was coated with a binary mixture of a biotinylated thiol (10 mol-%) and an OH-terminated thiol (90 mol-%) as the diluent molecule. The resulting self-assembled monolayer ($d_0 \approx 1.5$nm) was optimized for the binding of streptavidin from solution, leading to a monolayer of protein. Since the binding of streptavidin molecules leads to a measurable increase in the average layer thickness, and at the same time to an increase in the fluorescence intensity emitted form the incrementally growing surface coating, one can directly compare the two signals.

The kinetic scans are shown in Figure 4.4a, with a clear interruption in the layer formation process, due to the rinsing step with ethanol. Both the reflectivity and the fluorescence intensity remain constant thereafter. Figure 4.4b displays the reflectivity scans before and after the adsorption process. From the angular shift of the resonance curve induced by the streptavidin coating, an average layer thickness of $d = 4$ nm was obtained (n = 1.45 in the Fresnel simulations).

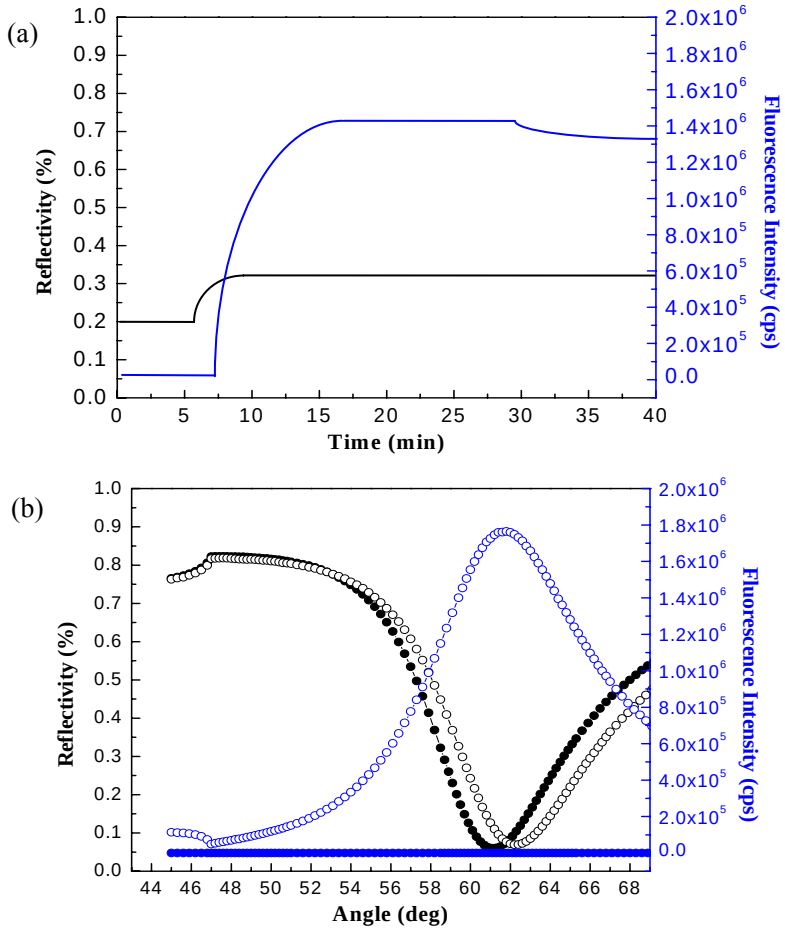

Figure 4.4: (a) Kinetic scan of the binding of cy3-streptavidin to surface immobilized Biotinylated SAM; (b) Full angular scanning curves before and after the binding of cy3-streptavidin.

The angular dependence of the fluorescence intensity, monitored simultaneously with the reflectivity curves, is also given in Figure 4.4b. Prior to the injection of the streptavidin solution, the fluorescence intensity was at the low level of the background counts (ca. 7000cps) but showed the expected strong intensity increase following the angular dependence of the resonant excitation of surface-plasmons.

4.4 Monitoring DNA hybridization reactions by surface –plasmon fluorescence spectroscopy

Once the general concept of using the resonantly enhanced optical fields of surface-plasmons propagating along a metal/dielectric interface for the excitation of chromophores at or near that interface, and of detecting the emitted fluorescence

photons has been established as a very sensitive approach for monitoring binding reactions, an obvious area of application for this novel method is in the field of bio-sensing.

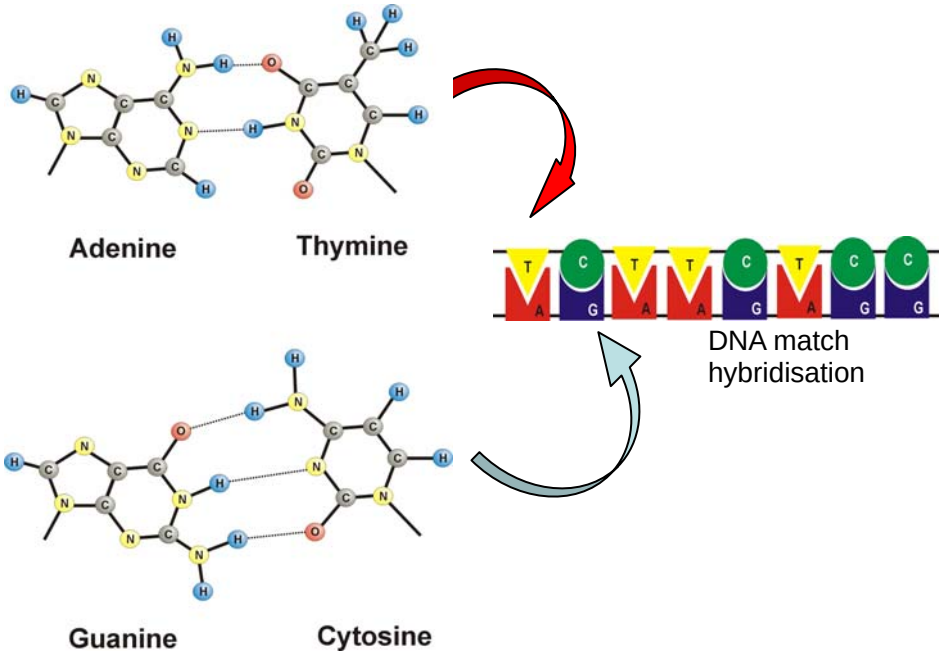

Figure 4.5: Schematic presentation of binding between complementary bases, adenine and thymine, and guanine and cytosine.

In the following, a few examples are given to demon the use of this technique to detect hybridization reactions between surface-attached oligonucleotide sequences as probe strands and complementary target strands approaching from solution and binding to probe via strong hydrogen bond formation between complementary bases, i.e., guanine and cytosine (G-C), and adenine and thymine (A-T).Despite its importance for gene-chip technology, little is known quantitatively about the details of these highly specific interactions. Intuitively, it is clear that the highly charged DNA backbone, which is composed of a phosphate-pentose sequence, couples strongly to the ionic parameters of the aqueous phase: pH, ionic strength, etc., which have a strong impact on the binding kinetics and the respective affinities.

Additionally, for hybridization reactions at surfaces, the interaction between neighboring strands may lead to Coulombic cross-talk and hence affect the observed binding reactions.

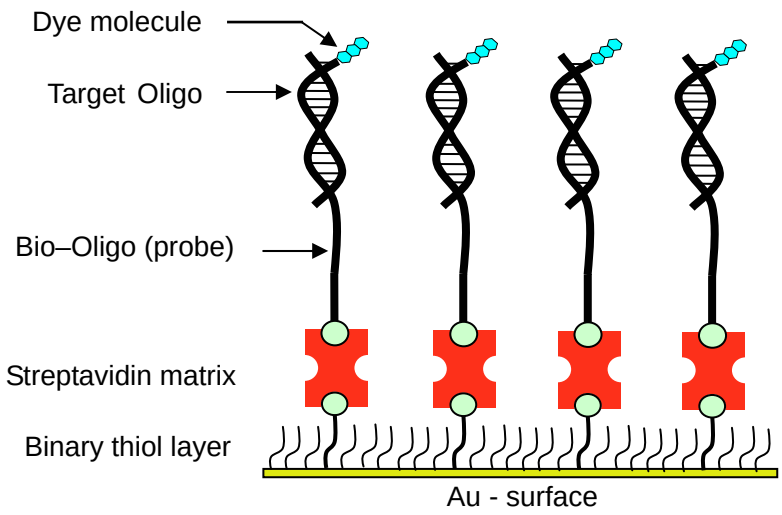

Figure 4.6: Schematic presentation of the sensor surface architecture: Onto an evaporated gold film a binary SAM of two thiols (OH-thiol and biotinylated thiol) was formed, which supported a streptavidin protein layer. Biotinylated oligonucleotides were finally immobilized and the hybridization reaction was monitored by measuring the fluorescence signal of he labeled target oligo.

With surface-plasmon field-enhanced fluorescence spectroscopy, one can have a tool-box that is very well suited to give experimental answers to these questions. Molecular architecture on the surface is schematically given in Figure 4.6 which describes the version of an unlabeled probe and a fluorescently labeled target strand. Upon hybridization, the number of surface-bound complements increases and so does the recorded fluorescence. By monitoring the fluorescence emission before, during, and after the binding of labeled target strands, one can gain information about kinetic rate constants and affinity values.

In the case of the DNA studies, catcher probe sequences used were also biotinylated and, thus could specifically bind to the free biding pockets of the streptavidin molecules at the sensor surface. In all cases of experiments with oligonuleotides, the

chromophores were coupled to the distal end of the respective chain, i.e., at the 3'-end in the case of a catcher and at the 5'-end for all targets.

(a) 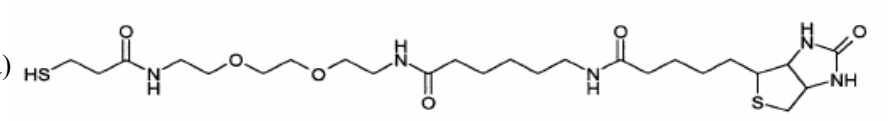

M_g = 575.80

(b) 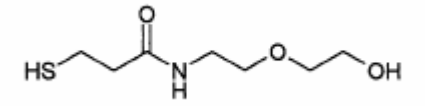

M_g = 193.27

(c) Probe sequence:

5'-biotin-TTT TTT TTT TTT TTT TGT ACA TCA CAA CTA-3'

(d) MM0 (no mismatch base with probe) target sequence:

3'- ACA TGT AGT GTT GAT -Cy3-5'

(e) MM1 (1 missmatch base with probe) target sequence:

3'- ACA TGC AGT GTT GAT -Cy3-5'

Figure 4.7: Structure formula of the biotinylated thiol (a) and OH-terminated thiol (b) employed in the preparation of the mixed self-assembled monolayer (SAM) which is capable of binding a monolayer of streptavidin. The base sequences of the employed probe oligonucleotide, MM0 (none mismatch base present) target oligonucleotide and MM1 (1 mismatch base present) target oligonucleotide are shown in (c), (d) and (e) respectively.

The chemical structures of all the (bio-) organic molecules employed are given in Figure 4.7. The OH-terminated thiol and the biotin-derivatized system were used in a 90:10 molar ratio for the assembly of a SAM from an aqueous solution. (cf. Section 4.3) The specific 15 mer base sequences of the catcher probe are separated from the biotin linker group by a sequence of 15 thymines acting as spacers. The used target sequences, fully complementary or with one mismatched base close to the middle of the sequence, were labeled either with Cy5 or Cy3 fluorophores. The Cy5 dye can be excited by employing the He:Ne laser at λ = 633 nm and emits photons at ca. λ = 650 nm. The Cy3 dye can be excited by employing the He:Ne laser at λ = 543 nm and emits photons at ca. λ = 570 nm.

The use of the streptavidin monolayer as a generic binding matrix with only one target strand bound, even at maximum loading, reduces the cross-talk between neighboring binding sites. However, it dilutes the analyte density at the interface to a mass density (equivalent to an optimal thickness) below the detectability limit for the usual surface-plamon spectroscopy.

Figure 4.8 and Figure 4.9 display examples of two typical experiments, each with a

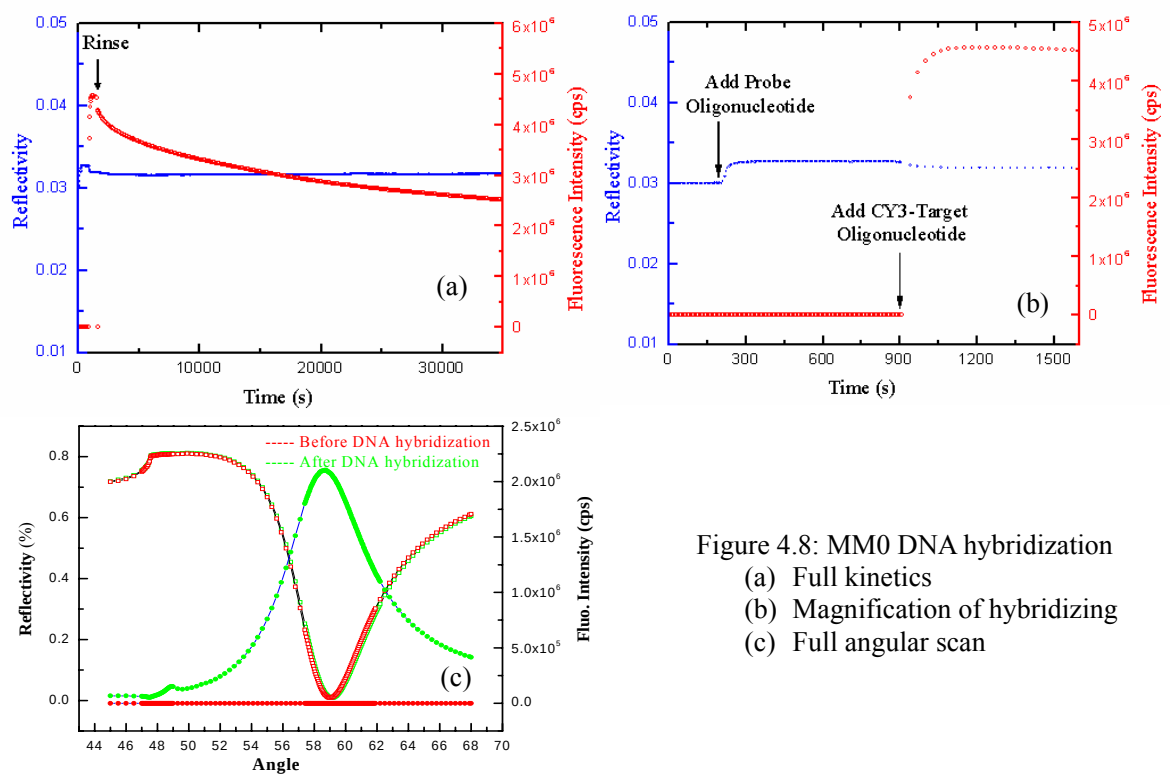

Figure 4.8: MM0 DNA hybridization
(a) Full kinetics
(b) Magnification of hybridizing
(c) Full angular scan

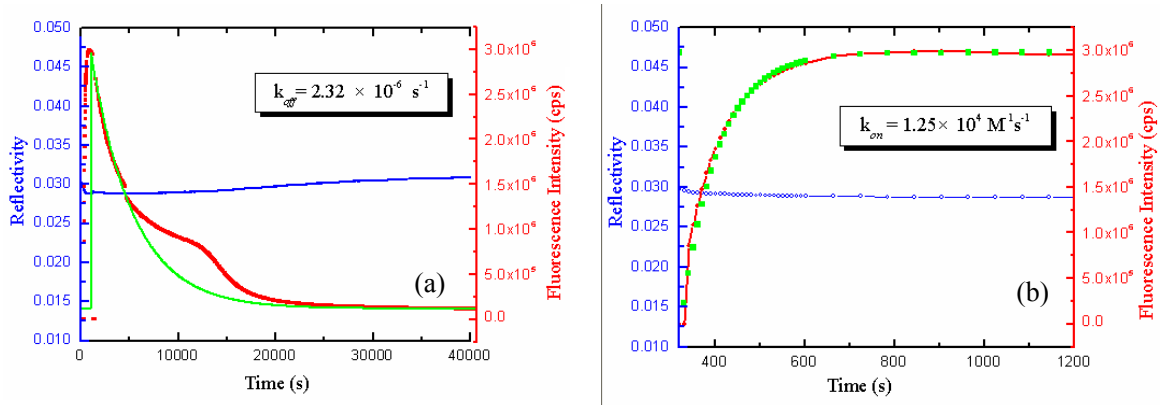

Figure 4.9: MM1 DNA hybridization. (a). Full kinetics;
(b). Magnification of hybridizing

kinetic scan taken before, during, and after the hybridization of a fluorescently labeled MM0 (no mismatch) and MM1 (with one mismatch) complementary 15 mer strand from solution to a surface-attached probe strand. The reflectivity, R, taken as a function of the angle of incidence, before hybridization is virtually identical to the curve taken after hybridization because of the little mass (optical thickness) added by the complement strands binding to a very dilute matrix of catcher probe with an upper limit of approximately one probe strand per ~ 40 nm^2 on the sensor's surface. The lateral density value is estimated according to the surface density of streptavidin. A streptavidin monolayer was formed by specific binding from solution to the biotin-sites at the surface. The obtained thickness of this layer of d = 4.0 nm (n = 1.45) corresponds to a surface coverage of ca. 53% (by SPR simulation), equivalent to a binding site density of $\delta \approx 1/ 24$ nm^2. One or two biotinylated probe oligos are expected to bind to one streptavidin molecule.

Consequently, the kinetic mode of SPR does not indicate any change during hybridization (see Figure 4.8b and Figure 4.9b). Since all of the complements carry a fluorophore that, upon hybridization, reach the high optical fields generated at the interface upon resonant excitation of surface-plasmons and hence emit fluorescence light, this fluorescence intensity, when taken as a function of time, contains the kinetic information of the hybridization reaction and can be analyzed in terms of the corresponding rate constants, k_{on}, for the association, and k_{off}, for the dissociation.

Figure 4.8 gives the results for MM0 hybridization: upon the addition of target solution the fluorescence intensity rises very rapidly and reaches a stable constant value. Rinsing with pure buffer affects the intensity only very little, leading to a very slow decrease with time. According to figure 4.8c, the fluorescence intensity, when measured before the addition of the complement, shows only a flat, angle-independent

background. After the complementary DNA strand binding, however, a strong fluorescence signal can be detected which shows the expected angle-dependence for surface plasmon field excitation: the emission intensity follows the angular resonance profile of the local field intensity calculated for this interfacial configuration. High photon counts, well in excess of 10^6 cps even after rinsing off any non-specifically adsorbed complementary strands, were observed. The corresponding angular scan of the fluorescence displayed in Figure 4.8c shows a very pronounced enhancement of the fluorescence intensity at the resonant excitation of surface-plasmons, with the typical angular displacement between the maximum emission and the minimum reflectivity.

A remarkably different behavior is found for the MM1 hybridization experiment (Figure 4.9). Again, the fluorescence rises to almost the same fluorescence intensity level after the addition of the labeled complement, though with a considerably reduced binding rate constant. However, if now the complement solution is replaced by pure buffer the fluorescence signal gradually decreases until after several hours no intensity can be detected any more.

All these kinetic curves can be described by a simple Langmuir model: the oligonucleotides in solution are in equilibrium with the ones bound to the sites at the interface, represented by the catcher probe oligos. Any change in the solution concentration, c_0, hence results in a change of the surface coverage, ϕ, of bound (hybridized) complements. Here, the two reaction rate constants, k_{on}, and k_{off} describe the whole process, and the reciprocal of affinity constant,

$$K_A = \frac{k_{on}}{k_{off}} \tag{4.2}$$

$1/K_A$, is the half-saturation concentration, i.e. the solution concentration at which one half of the maximum probe sites are occupied. The two types of experiments presented in Figure 4.9 are then described by

$$I_{fl}(t)=I_{max}[1-\exp(-(c_0 k_{on}+k_{off})(t-t_0))] \quad (4.3)$$

for the adsorption (hybridization) following a step-wise increase of the solution concentration from 0 to ∞, and

$$I_{fl}(t)=I_{max}\exp[-k_{off}\,(t-t_0)] \quad (4.4)$$

for the desorption upon decreasing c_0 again to ≈0 by rinsing buffer through the cell.

With these simple expressions for the time-dependence of the fluorescence change, data of Figure 4.9 could be very well fitted, giving the affinity constant $K_A = \frac{k_{on}}{k_{off}} = 5.4\times10^9\ \mathrm{M}^{-1}$. The MM1 kinetic data at this point are considered to be reliable in a quantitative sense: the agreement between the measured time-dependent fluorescence intensities and the simulated kinetics is excellent over the whole experimental range.

4.5 Surface-plasmon field-enhanced microscopy and spectrometry

4.5.1 Introduction

Similar to the nature of surface-plasmon being surface-bound light has led to the introduction of surface plasmon microscopy (SPM) [28, 29], following section will show that this novel concept of surface plasmon fluorescence techniques can also be applied to microscopic and spectrometric formats for the characterization of laterally structured samples.

The experimental setup used for this work is a direct extension of the one described in

earlier works on surface-plasmon fluorescence spectroscopy [30, 31]. It is based on the principle of detecting fluorescence light from dye-doped latex particles located

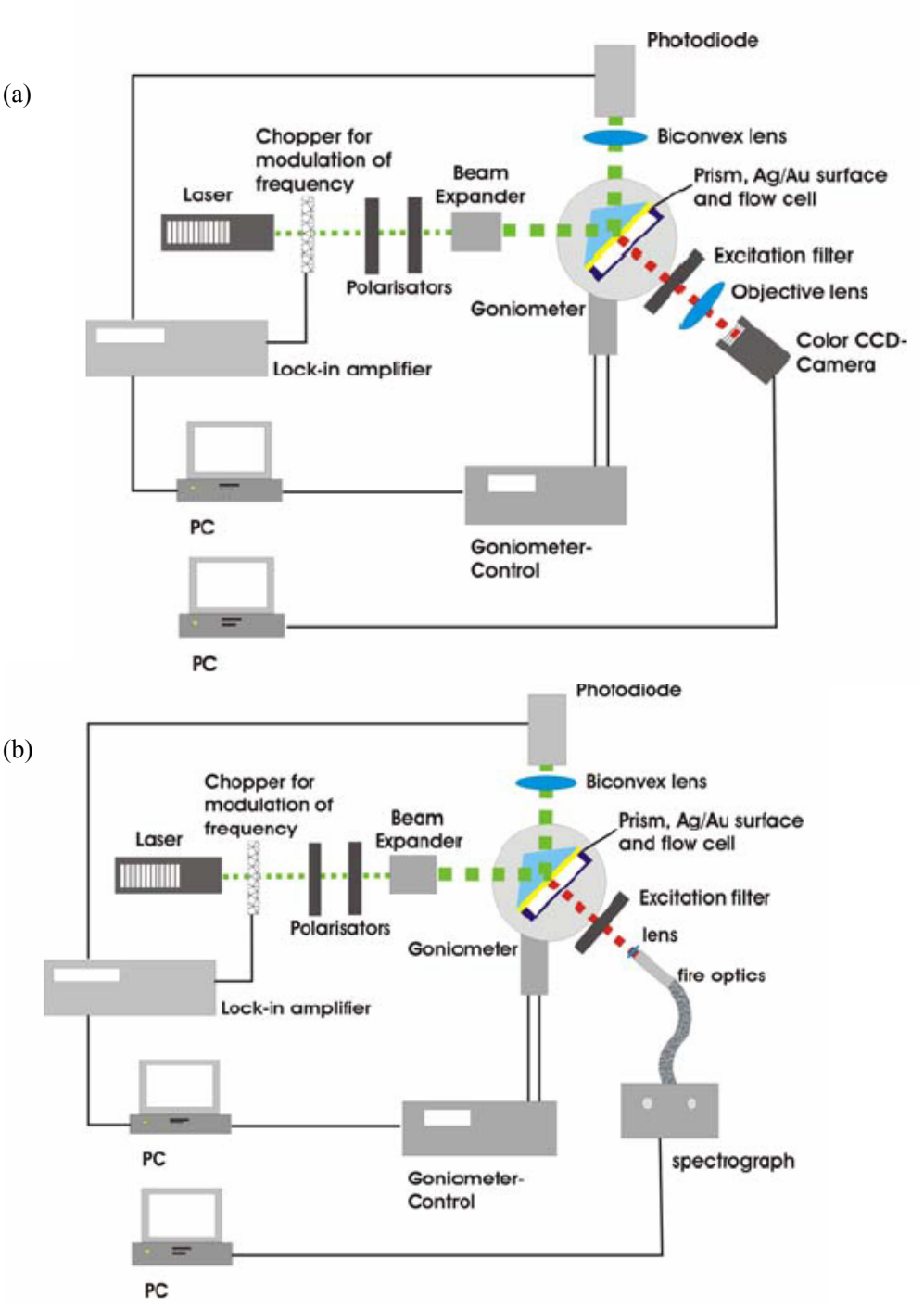

Figure 4.10: Schematic experimental setups for (a) surface-plasmon field-enhanced fluorescence microscopy and (b) surface-plasmon field-enhanced fluorescence spectrometry using fiber optics and s spectrograph.

near the metal/dielectric interface, excited by the resonantly coupled surface-plasmon modes propagating along this interface [32].

A simplified schematic diagram showing the combination setups that allow for recording of surface-plasmon field-enhanced fluorescence microscopy and surface-plasmon field-enhanced fluorescence spectrometry with an optical fibre, is given in Figure 4.10a and 4.10b. A light beam from a HeNe laser (Uniphase 1 mW, $\lambda = 543$ nm) is controlled in its intensity and polarization by two polarizers and then passes a beam-expanding unit. The light is coupled via a high-index prism (LaSFN9) in this Kretschmann configuration to the (Ag/Au) metal-coated substrate which is index-matched to the prism via a kind of high refractive immersion oil (Cargille, USA). A flow cell (volume $V = 100$ μL) is used for on-line recordings of hybridization reactions. The reflected light is imaged via a biconvex lens onto a photodiode. Sample cell and camera are mounted to a two-stage goniometer such that θ-2θ angular scans can be performed in the normal reflection mode of surface-plasmon spectroscopy.

For the fluorescence microscopy, a particularly sensitive color CCD camera (Kappa optoelectronics, Gleichen, Germany) is mounted to that part of the goniometer that rotates the sample cell (θ) thus ensuring that the camera always looks at a fixed angle normal to the substrate surface. To avoid the collection of scattered and transmitted laser light, an excitation filter (Omiga Opticals Inc, USA) is placed between the flow cell and the CCD camera. The software package KAPPA Image Base Control (Kappa optoelectronics, Gleichen, Germany) allows for the recording of the fluorescence images. The camera is operated at an internal temperature of $T = 25°C$ and with an integration time of $\Delta t = 20$ sec.

For the surface-plasmon field-enhanced fluorescence spectrometry the experimental setup is modified in such a way, that the color CD camera is exchanged by a fiber optics cable collecting the fluorescent light, which passes through the excitation filter and is focused by a lens sitting in front of the fiber optics collection head. The

fluorescence light is then remitted to a MS125 spectrograph unit (Thermo Oriel, Stratford, CT, USA). Data collection and processing are performed with a PC running the software "Andor MCA V2.62" from Andor Technologies (Belfast, Northern Ireland).

4.5.2 Experimental preparation

4.5.2.1 Probe DNA oligos and quantum dot conjugation of target DNA oligos

The probe and target DNA sequences used in this study are shown in Table 4.1. All oligonucleotides had a biotin unit attached at the 5' end. In addition to 15 thymine residues used as a spacer, the sequences exhibited 15 nucleobases as the particular recognition sequence. The recognizing nucleotides of P1 and P2 were fully complementary with the 15 bases located at the 3'-end of T1 and T2. The biotin

Table 4.1: (a) Nucleotide sequences of the probe and target single stranded DNAs used for the experiments; (b) Possible hybridizations.

(a)

Name	Nucleotide Sequence
P1	5'-Biotin-TTT TTT TTT TTT TTT GCA CCT GAC TCC TGT-3'
P2	5'-Biotin-TTT TTT TTT TTT TTT TGT ACA TCA CAA CTA-3'
P3	5'-Biotin-TTT TTT TTT TTT TTT TAG TTG TGA TGT ACA-3'
T1	5'-Biotin-TTT TTT TTT TTT TTT ACA GGA GTC AGG TGC-3'
T2	5'-Biotin-TTT TTT TTT TTT TTT TAG TTG TGA TGT ACA-3'

(b)

Possible hybridizations	Number of miss-match bases
P1◄►T1	MM0
P1◄►T2	MM14
P2◄►T1	MM14
P2◄►T2	MM0
P3◄►T1	MM14
P3◄►T2	MM11

anchor group attached to the probe and target oligonucleotides facilitated their immobilization to the surface bound streptavidin monolayer either on a sensor surface or on a quantum dot.

The conjugation of target DNA oligonucleotides to the quantum dots was prepared as follows: 100 µL Qdot™ streptavidin conjugates (2 µM) were diluted to a volume of 1.8mL by adding quantum dot reaction buffer. The reaction mixture was completed by the addition of 200 µL oligonucleotides in $H_2O_{bidest.}$ (20 µM). The mixture was stirred in the dark for 2 h at RT. The excess of non conjugated oligonucleotides was removed by a gradual concentration of the reaction mixture with 30 kDa Nanosep® centrifugal concentrators and a subsequent resuspension with PBS buffer. This procedure also exchanged the quantum dot reaction buffer with a PBS buffer, which was suitable for the performed hybridization experiments. The quantum dot – DNA conjugates were stored in PBS buffer at 4°C in the dark.

4.5.2.2 Cy3, Cy5 and QDs -labeled DNA grating preparation upon hybridizing

The fabrication procedure of the photo pattern is schematically shown in Figure 4.11. Firstly, a monolayer of OH-terminated thiol is self-assembled on the silver/gold (37/8nm) surface. Then a copper mesh (150 or 100 mesh) is placed on top and irradiated by UV light for about 40mins. The oxidized thiol molecules are rinsed off and again a binary mixed monolayer of biotinylated thiol derivative and OH-terminated thiol is self-assembled. On top of the binary mixed monolayer are streptavidin monolayer, probe oligonucleotide and at last the labeled target oligonucleotide assembled. The first three steps were done outside the flow cell and the last three steps were done within the flow cell.

The main steps to get the images include: Angular scans in order to locate the

approximate coupling angle. The sample was then set at this angle to excite surface plasmons and further excite dyes or QDs. An excitation filter of 543 nm was used to block the scattered light from surface plasmons.

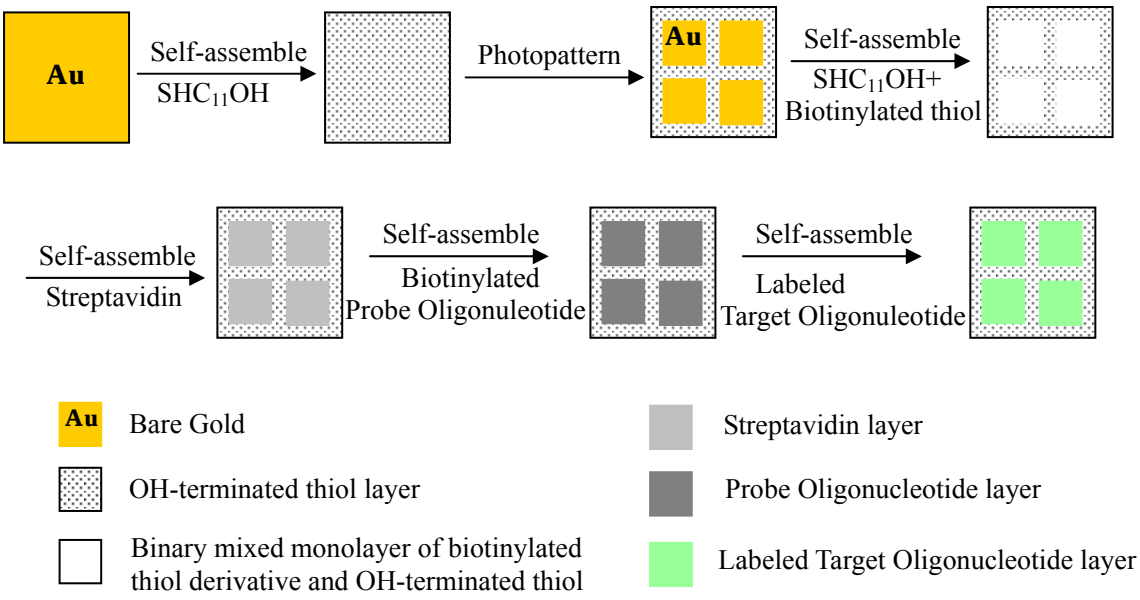

Figure 4.11: Schematic diagram of the preparation of photopattern surface.

4.5.2.3. Surface preparation and micro-array fabrication

Here, SPFM and SPFS were used to realize the parallel detection of hybridization reactions to a whole micro array of individual sensor spots by using a highly sensitive color CCD camera as the recording element. The camera takes time-dependent images of the fluorescence intensities emitted from each sensor element arranged on the chip surface in a matrix format using a microarray chipwriter preparation protocol. This way, a large number of individually functionalized spots can be monitored simultaneously. For simplicity, the studies were limited to an array of 4×3 spots of 3 different probe oligonucleotide sequences. The preparation of the SPFM and SPFS surfaces emanated from LaSFN9 glass slides, which were coated with a mixed Ag/Au (37/8 nm) metal layer. Firstly, a mixed self-assembled monolayer (SAM) of a

biotinylated thiol derivative and a short chain OH-terminated thiol used as a diluent at a mixing ratio of 1:9 was assembled at the Ag/Au substrates, generating a binding matrix optimized for the formation of a streptavidin monolayer via the specific recognition to the biotin moieties. The streptavidin monolayer was then created on top of this SAM by incubation of the surfaces with 500nM streptavidin in PBS. The bound streptavidin exposes biding sites to the aqueous phase of the cuvette which allows for the assembly of an oligonuleotide catcher probe layer.

For the preparation of a micro array sensor, 12 microspots of biotinylated probe DNA oligonucleotides were spotted on the center of this streptavidin monolayer surface with a pitch of 350μm between the spots by using an ESI SMA^{TM} Arrayer. The micro spotting is thereby accomplished by direct surface contact between the printing substrate and a delivery module that contains an array of pins that serve to transfer the biochemical samples to the surface. Once the microarrayed slides are freshly prepared, they will be kept in a desiccator until used.

The solution for the analysis of target DNA sequences contained the corresponding QD-DNA conjugates, QD_{565}-T1 and QD_{655}-T2. The QD conjugated target DNA sequences have 15 nucleobases complementary to their respective probe strands P1 and P2. Both quantum dot populations, QD_{565} and QD_{655} respectively, could be excited with a green HeNe laser line (λ = 543 nm) and the emitted fluorescence photons were recorded at λ = 565 nm and λ = 655 nm.

The 12 microspots of biotinylated probe DNA oligonucleotide are arrayed on the center of the streptaviding monolayer surface with a pitch of 350 between the spots. The arrangement of the 12 spots is schematically depicted in Figure 4.12.

The solution for analysis contains the corresponding target strands, QD_{565nm}-

conjugated T1 and QD_{655nm}-conjugated T2, which are fully complementary with their respective probe strands P1 and P2. Both of QD_{565nm} and QD_{605nm} could be excited by the green HeNe laser line (λ = 543 nm) and emitted fluorescence photons recorded at 565 nm and 655 nm.

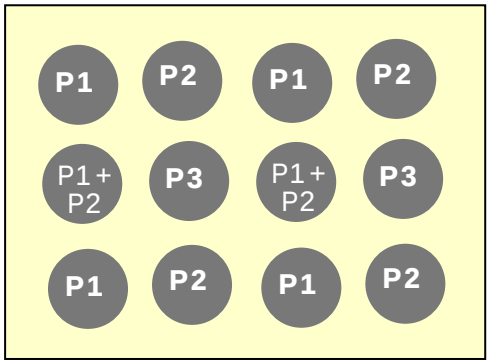

Figure 4.12: Surface Plasmon field enhanced fluorescence images preparation: Schematic arrangement of different probe DNA spots on the gold/SAMs micro array sensor surface.

4.5.3 Experimental Results

4.5.3.1 Characterization of Cy3-labeled DNA target strand hybridizing to the surface-stabilized DNA probe strand in a grating format

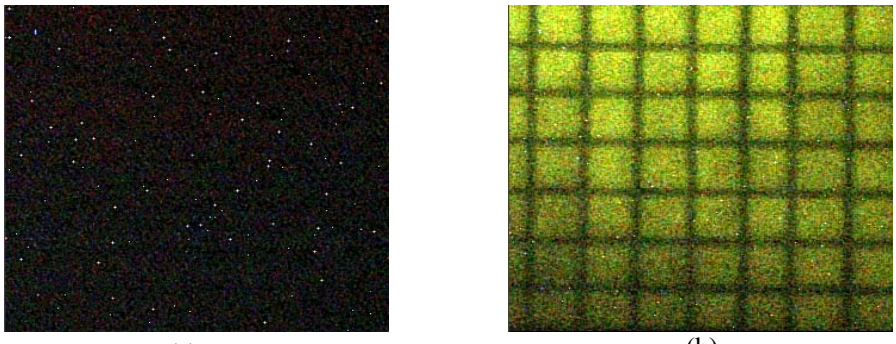

(a) (b)

Figure 4.13: Images from SPFM before (a) and after (b) the adding of Cy3-labeled target DNA solution.

Fabrication process of surface grating structure is schematically given in Figure 11. On the areas of dividing lines is self-assembly monolayer of OH-terminated thiol and on the areas of squares is self-assembly binary mixed monolayer of biotinylated thiol

derivative and OH-terminated thiol. On top of the binary mixed monolayer are streptavidin monolayer and biotinylated probe oligonucleotide. Areas of squares were functioned with probe oligos and were expected to have hybridization reactions.

Figure 4.13 shows the results of Cy3-labeled target hybridization obtained by SPFM. An excitation filter of 543 nm was used to block the light from surface plasmons. (a) is the image of the surface before introducing target oligos. No fluorescence image can be observed at all even though the integration time has been set quite long.

Only 5mins after introducing Cy3-labeled target oligos, the grating image of surface

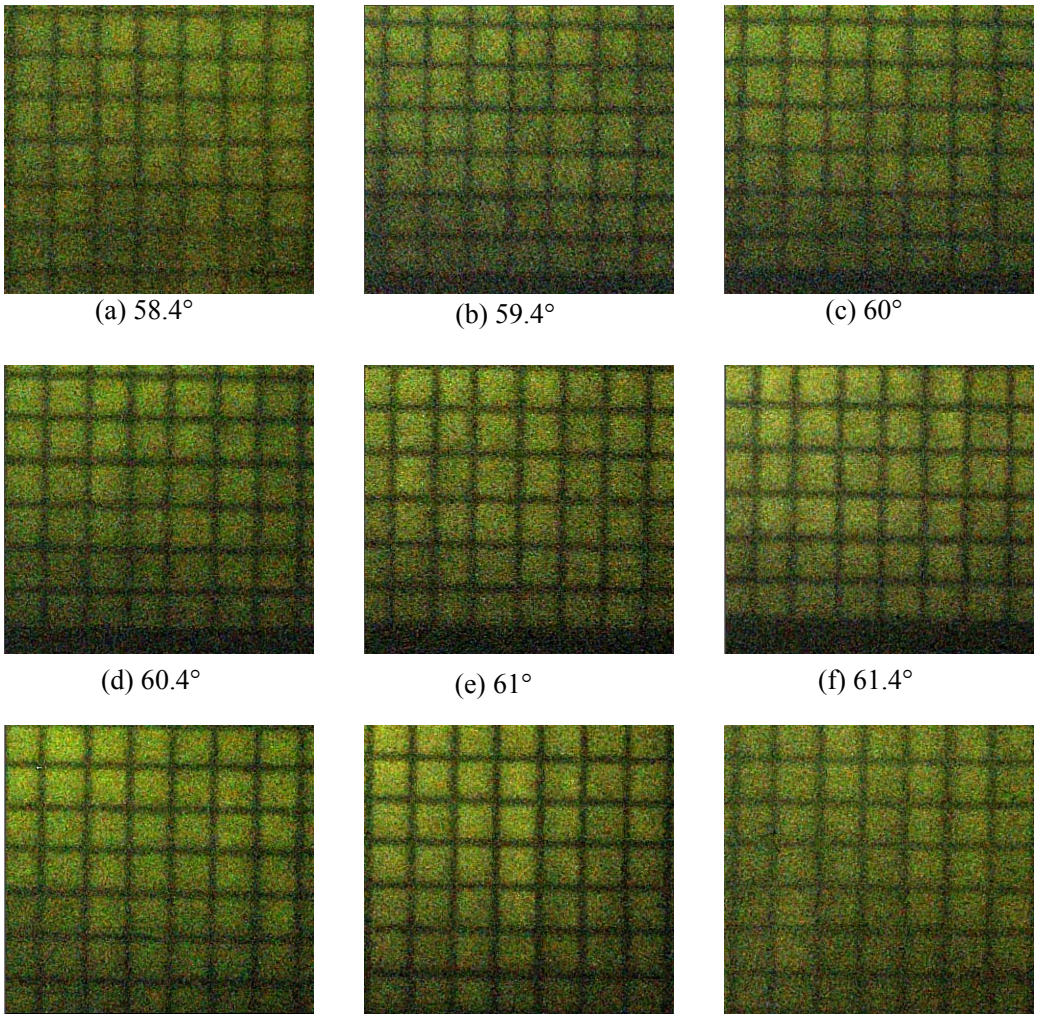

(a) 58.4° (b) 59.4° (c) 60°

(d) 60.4° (e) 61° (f) 61.4°

(g) 62° (h) 62.4° (i) 63°

Figure 4.14: The grating images with same integration time but at different angles.

can be seen with the dividing lines black and squares bright. As predicted, complement hybridization from solution to surface-attached probe-oligonucleotides has been observed. As a negative contract, areas of dividing lines remain dark, indicating no hybridization is undergoing at these areas.

The series of images in Figure 4.14 are with the same integration time of 8s but at different incoming angles from 58º to 63º, with the resonance angle obtained from the normal SPR angular scan being at around 61.4. It seems that the image of DNA pattern can be gained within a quite large angular scope, which is in perfect agreement with the fluorescence intensity distribution obtained from the angular scan of surface plasmon fluorescence spectroscopy.

4.5.3.2 Characterization of self-prepared QDs grating

It is interesting to observe the emission of excited QDs by fluorescence microscopy. The aim of using pattern is just to provide something to be focused by the microscopy. Otherwise, it is difficult to locate the area with QDs.

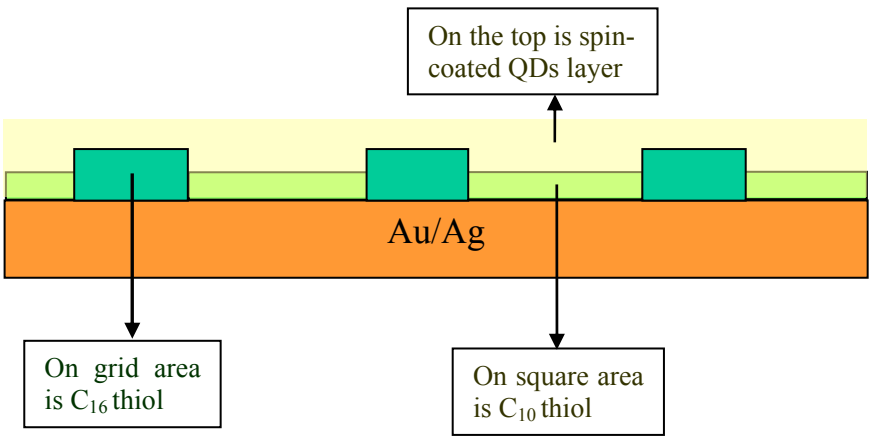

Figure 4.15: Quantum Dot grating-patterned surface architecture. The 574 nm QDs were prepared by our own group. Detailed conditions include:
Pattern: C_{16} thiol SAM on grid, C_{10} thiol SAM on square
QDs (584nm): in toluene (freshly prepared)
Spin-coating speed 1: 1000 rpm, 6 s
Spin-coating speed 2: 3000 rpm, 40 s

Pattern was prepared on gold/silver surface by a copper grid and UV light, the process of which is similar to DNA grating pattern described before. On the grid is C_{16} thiol monolayer and on the square area is a C_{10} thiol monolayer. So the two area have different thickness and different coupling angle, which is crucial to get the images by both SPM and fluorescence microscopy. On top of the thiol layer pattern a QDs layer is spin-coated.

These are important steps to get the images. Firstly, taking an angle-scan curve is crucial in order to know the average coupling angle of the patterned area. Then move to the angle to excite QDs by surface plasmon.

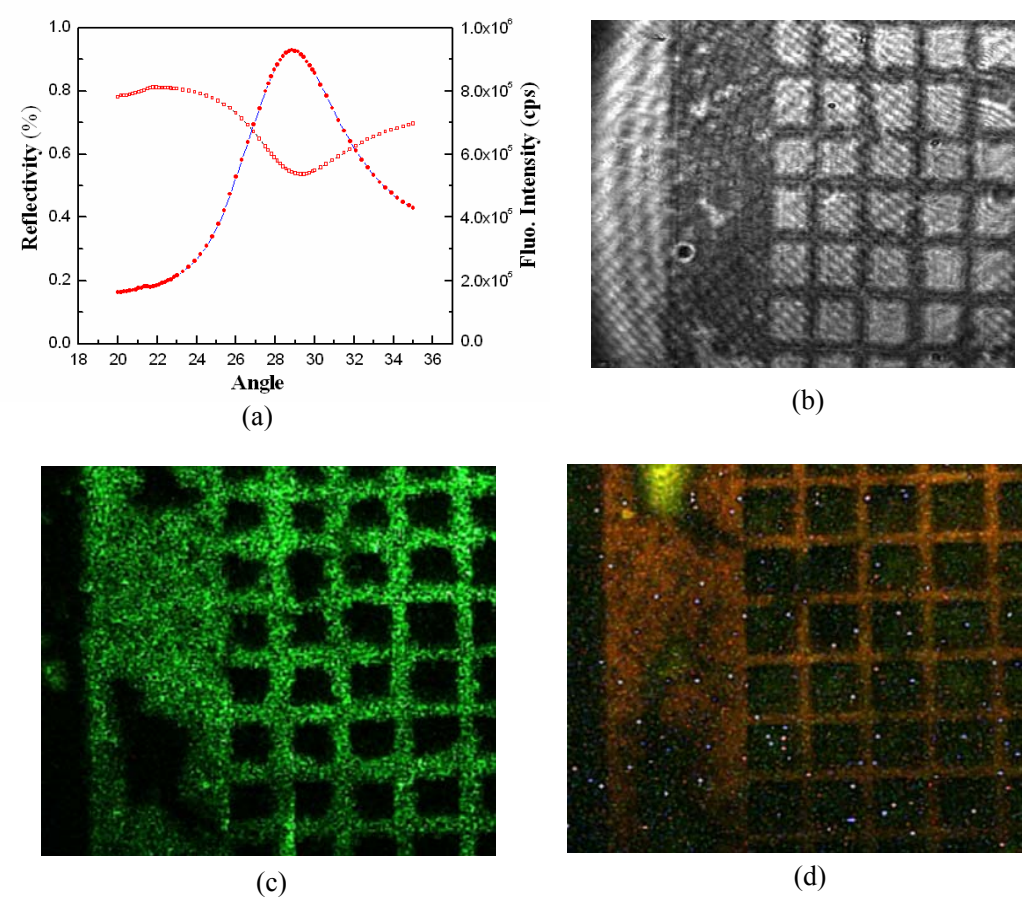

Figure 4.16: Measuring results of QDs grating. (a) Angular scan curve from SPFS (spectroscopy); (b) Image from SPM; (c) Image from SPFM without filter; (d) Image from SPFM with 543 nm excitation filter.

Figure 4.16 (a) shows the angular scan curve of the coated surface. The fluorescence intensity is about 8105cps. The coupling angle is about 28.7º. The whole range angle scan from 20º to 80º shows only one fluorescence excitation peak.

Figure 4.16 (b) is the image of the grating surface obtained by SPM at 29º. The dark areas refer to the C_{16} spacer and the bright areas refer to the C_{10} spacer. Here, at the coupling angle of grid area, the image should show a dark grid with bright square. Images in (c) and (d) were taken by SPFM. The image (c), taken without any filter, comes directly from surface plasmon and scattered laser light, whose wavelength and color are the same as the green laser. Image (d) was taken with the 543 nm excitation filter which blocks the laser light and only transmits fluorescence light from the sample surface. The light in image (d) originates from fluorescence emission of the quantum dots.

4.5.3.3 Quantum dot-labeled DNA grating upon hybridization

This part is concerned with the use of quantum dots to label target DNA strand. There are good reasons to use quantum dots in our system. Quantum Dots are small inorganic nanocrystals that possess unique luminescent properties. QDs have the potential to become a new class of fluorescent probes for many biological and

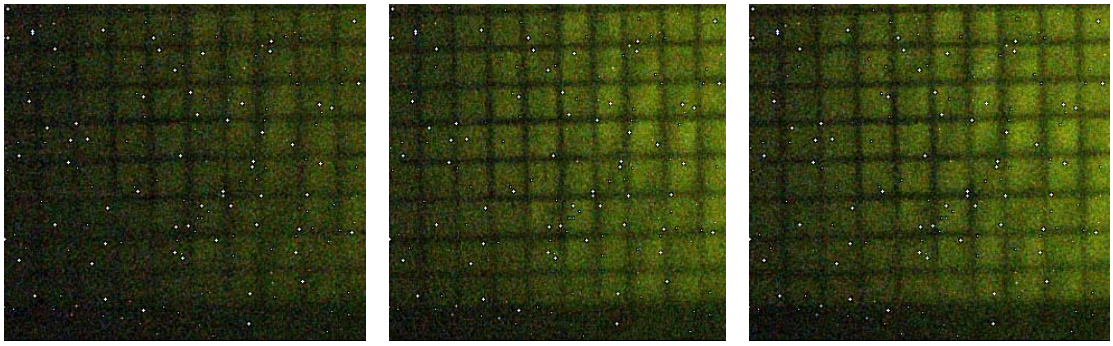

(a) Hybridizing for 20min

(b) Hybridizing for 35min

(c) Hybridizing for 55min

Figure 4.17: Images from SPFS at different hybridizing time after the adding of QDs-labeled target DNA solution.

biomedical applications. As fluorescent probes, QDs have several advantages over conventional organic dyes. Their emission spectra are narrow, symmetrical, and tunable according to their size and material composition, allowing closer spacing of different probes without substantial spectral overlap. They exhibit excellent stability against photobleaching. They display broad absorption spectra, making it possible to excite all colors of QDs simultaneously with a single excitation light source [33, 34].

The three images in Figure 4.17 are with the same integration time of 18s but taken at different hybridization times. Compared with the Cy5 or Cy3 labeled DNA, quantum dots- labeled target DNA need much longer time to bind to probe DNA. The reason might be that quantum dots, with a diameter of about 8nm, greatly influence the movement of DNA molecules. But anyway, after 55min hybridization, with integration time of 18 s, the image of the grating pattern can be clearly seen.

4.5.3.4. Hybridization detection of quantum dot conjugated DNA by SPFS (spectroscopy format)

Here, the parallel detection of hybridization reactions to a whole micro array of individual sensor spots was conducted by using SPFS spectrometry techniques. The experimental preparation has been described in 4.3.2.3.

As the presented work is based on the technique of surface plasmon enhanced fluorescence spectroscopy, experiments showing the suitability of QD-DNA conjugates for this technique had to be conducted as a basic step.

The conjugation of CdSe/ZnS core-shell quantum dots to DNA was done via the extreme strong streptavidin/biotin interaction. For this purpose streptavidin coupled QDs were purchased from Q-Dots Inc. 5-biotinylated single stranded target DNA sequences were applied to these QDs. After removal of non bound excess DNA via

ultra filtration, pure QD-DNA conjugates could be attained. By a combination of fluorometry for the determination of the QD concentrations and UV spectroscopy for the quantitative determination of the attached DNA, a rough characterization of the conjugates showed a ratio of about 10 DNA sequences being coupled to one quantum dot.

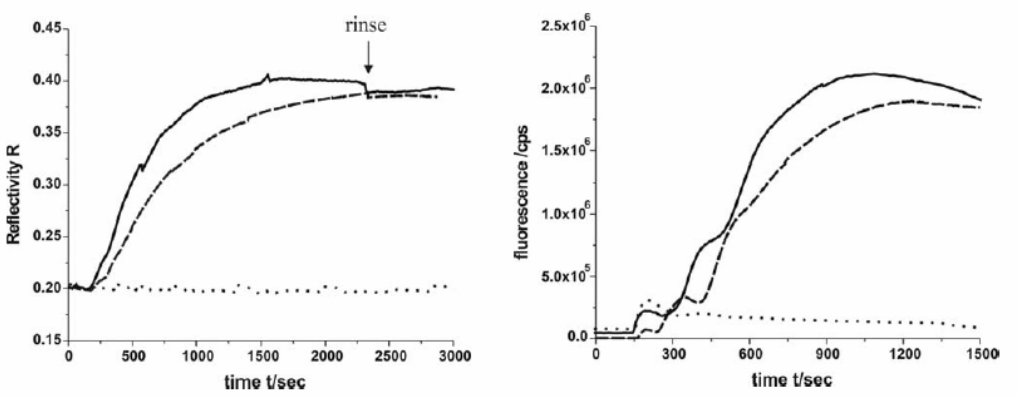

(a) (b)

Figure 4.18: SPR (a) and SPFS (b) measurements of the hybridization reactions of QD_{655}-T1 with P1 (full curve), QD_{565}-T2 with P2 (dashed curves) and QD_{655}-T1 with a surface containing no probe DNA (dotted curve).

For the basic SPR and SPFS experiments with these QD-DNA conjugates samples of 20 nM QD-DNA conjugates in PBS were applied to the sensor surfaces in a standard SPFS setup. The results of these experiments are summarized in Figure 4.18. Figure 4.18(a) shows the SPR signals generated by hybridizing two different QD-DNA conjugates (QD_{655}-T1 and QD_{565}-T2) with their corresponding complementary probe DNA matrices (P1 and P2). A clear hybridization of QD-conjugated target DNA with the respective surface bound probe DNA can be seen. The height of the hybridization signal ($\Delta R = 0.18$ for QD_{565}-T2/P2 and $\Delta R = 0.20$ for QD_{655}-T1/P1), which would be about $\Delta R = 0.015$ in case of a single 30mer target DNA strand shows that a relatively large mass must be attached to the target DNA strand. The unspecific binding of QD-DNA conjugates with the bare surface matrix of the sensor and with non-

complementary probe DNA strands is very low.

Once the target DNA bound QDs are close enough to the sensor surface to be within the evanescent tail of the surface plasmon field, the fluorescence signal is generated as shown in Figure 4.18(b). Both QD-DNA conjugates show a high fluorescence signal for the case of specific probe/target DNA hybridizations. A fluorescence signal derived from unspecific interactions between the QD-DNA conjugates and the sensor surface is visible but low enough to allow for a clear discrimination of specific and unspecific binding events.

By combining both the reflectivity and the fluorescence signals, which result from a specific binding of complementary probe DNA to its corresponding QD-target DNA conjugate, the suitability of the described conjugation system for its use in SPR and SPFS could be demonstrated.

4.5.3.5. Hybridization detection of quantum dot conjugated DNA by SPFM (microscopy format)

Following these basic experiments, it was investigated the possibility to confer the system to a surface plasmon enhanced fluorescence microscopy (SPFM) setup. The sensor surface was assembled as described above in a 3×4 micro array format. The arrangement of the resulting 12 spots and there composition of different probe DNA sequences is schematically depicted in Figure 4.12 and Table 4.1. Row 1 and 3 of the array consist of 4 spots of alternation P1 and P2 while row 2 holds spots with a 1/1 mixture of P1+P2 and spots with P3, a probe DNA sequence which serves as a negative control because of its 14 mismatching bases for T1 and T2 DNAs.

After the mounting of the prepared probe oligo micro array slide on the SPFM setup, there are still several steps to take before obtaining images. Firstly, a full SPR angular

scan with PBS buffer as medium is necessary in order to locate the rough resonance angle of the patterned area. The sample slide is then illuminated at this angle in order to excited surface plasmons at the interface between the slide surface and the buffer medium. After positioning the sensor array near the SPR reflectivity minimum, QD-DNA conjugates were injected to the system.

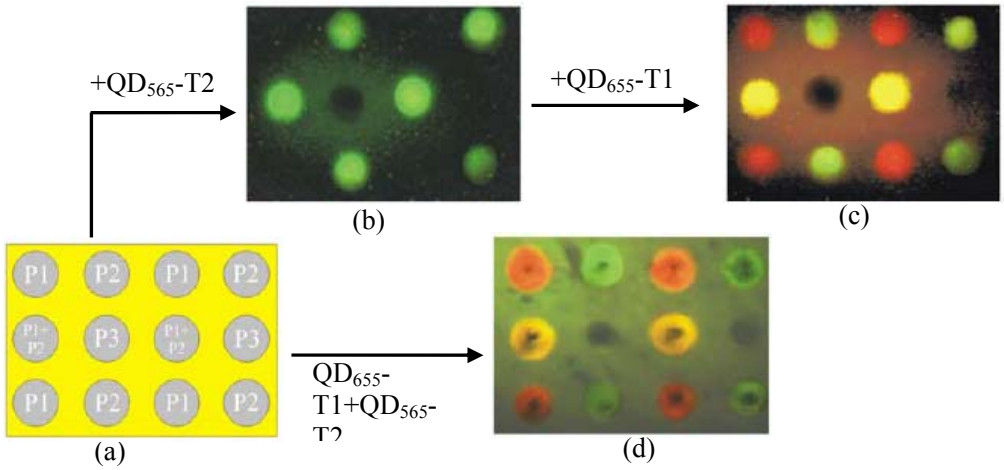

Figure 4.19: SPFM images of micro array sensor surface: (a) Schematic arrangement of different probe DNA spots on the gold/silver/SAMs micro array sensor surface; (b) and (c) Sequential injection of 20nM PBS solution of QD_{565}-T2 and QD_{655}-T1 conjugates, respectively, into the flow cell (2 min injection time each; integration time of the color CCD: 20sed); (d) Injection of a 1:1 mixture of a 20nM PBS solution of QD_{565}-T2 and QD_{655}-T1 (2 min injection time each; integration time of the color CCD: 20sed)

In a first series of experiments the injection of a 20nM PBS solution of each of the two QD-DNA samples was done sequentially with a rinsing step in between. The upper path in Figure 4.19 shows the results one obtains from this step by step addition experiment. The injection of QD_{565}-T2 resulted in the observation of green fluorescent spots, which were located exactly at the positions where the P2 target DNA and P1+P2 mixture were spotted on the micro array sensor (Figure 4.19b). All spots containing no P2 probe DNA remained dark. Subsequently, the second QD-DNA sample, QD_{655}-T1, was applied to the system. The red fluorescence of the QD_{655} could now be observed at the spots where P1 was located on the micro array (Figure 4.19 c).

Furthermore, the spots containing P1+P2 changed their color from green to yellow. This is due to the RGB color addition of the green fluorescence caused by P2 hybridized QD_{565}-T2 and the red fluorescence arising from P1 hybridized QD_{655}-T1. Only the spots with P3, the probe DNA that is fully mismatching with both, T1 and T2, did not show any fluorescence signal. A slight red fluorescent background signal could be seen in this experiment, which originated from QDs excited by the evanescent surface plasmon field in the bulk phase. However, even without rinsing this background fluorescence is low enough to allow for a clear visualization of the selective hybridization reaction of both QD-DNA populations with their respective array bound complementary probe DNA sequences.

In a second set of experiments, a 1:1 mixture of both QD-DNA conjugates was injected into the flow cell. After a reaction time of 2min the image given in Figure 4.18 d could be seen. Equivalent to the step by step addition of the two QD-DNA conjugates each target DNA hybridized with its complementary probe DNA-sequence on the corresponding micro array spot of the sensor surface. Even the P1+P2 probe DNA mixtures showed the same RGB color addition of green and red fluorescence resulting in a yellow signal spot. This experiment showed clearly, that a decomposition of mixed QD-DNA populations on the micro array and the qualitative analysis of the single conjugates via SPFM can be achieved.

4.5.3.6. Hybridization detection of quantum dot conjugated DNA by SPFS (Spectrometry format)

In addition to the qualitative SPFM analysis of QD-labeled target DNA sequences a more quantitative approach was implemented by exchanging the color CCD camera, which serves as an image generating component in the SPFM setup with a fiber-optics

coupled spectrograph. Using this setup the excitation of surface bound fluorescently labeled analytes can be combined with the spectral resolution of the fluorescence signal. Thus a simultaneous detection of diverse fluorophores with different emission wavelengths is possible, as is the case of using different quantum dots.

In our case a fiber-optics coupled spectrograph was used for the simultaneous detection of the QD_{565} and QD_{655} fluorescence on the above described micro array sensor surface. After setting the angle of incidence for highest fluorescence intensity a mixture of QD_{565}-T2 and QD_{655}-T1 (20 nM in PBS) was rinsed through the flow cell and, hence, brought in contact with the probe-functionalized micro array for 10 min. After this time no further change in the intensity of the fluorescence signal could be observed.

The spectrally resolved fluorescence signals are displayed in Figure 4.20a. As can be seen, the fluorescence signal can be split up into two bands with emission wavelengths of λ = 565 nm (QD_{565}-T2) and λ = 655 nm (QD_{655}-T1), respectively. The wavelength λ = 543 nm of the laser source, used for the excitation of the whole SPFS system, contributes only a negligible peak in the detected signal. The difference in the two fluorescence intensities is due to a slightly higher fluorescence quantum yield of the green fluorescent QD_{565} at the excitation wavelength λ = 543nm. Next, the fluorescence signal was recorded over a spectral range from λ = 500nm to λ = 700nm starting from an angle of incidence of θ = 45° up to an angle of θ = 75° in 10 intervals of $\Delta\theta$ = 2.5°. Figure 4.20b shows some of the spectra thus obtained. Plotting the highest intensities for both wavelengths, i.e., λ = 565 nm and λ = 655 nm, respectively, against the angle of incidence results in the angular fluorescence intensity scans given in Figure 4.20c. A comparison of these excitation scans with the ones obtained from a SPFS (spectroscopy format) angular scan with a P1/QD_{655}-T1 hybrid (Figure 4.20d)

shows the exact conformance of the angle with the highest total fluorescence signal reached at θ = 61.55°.

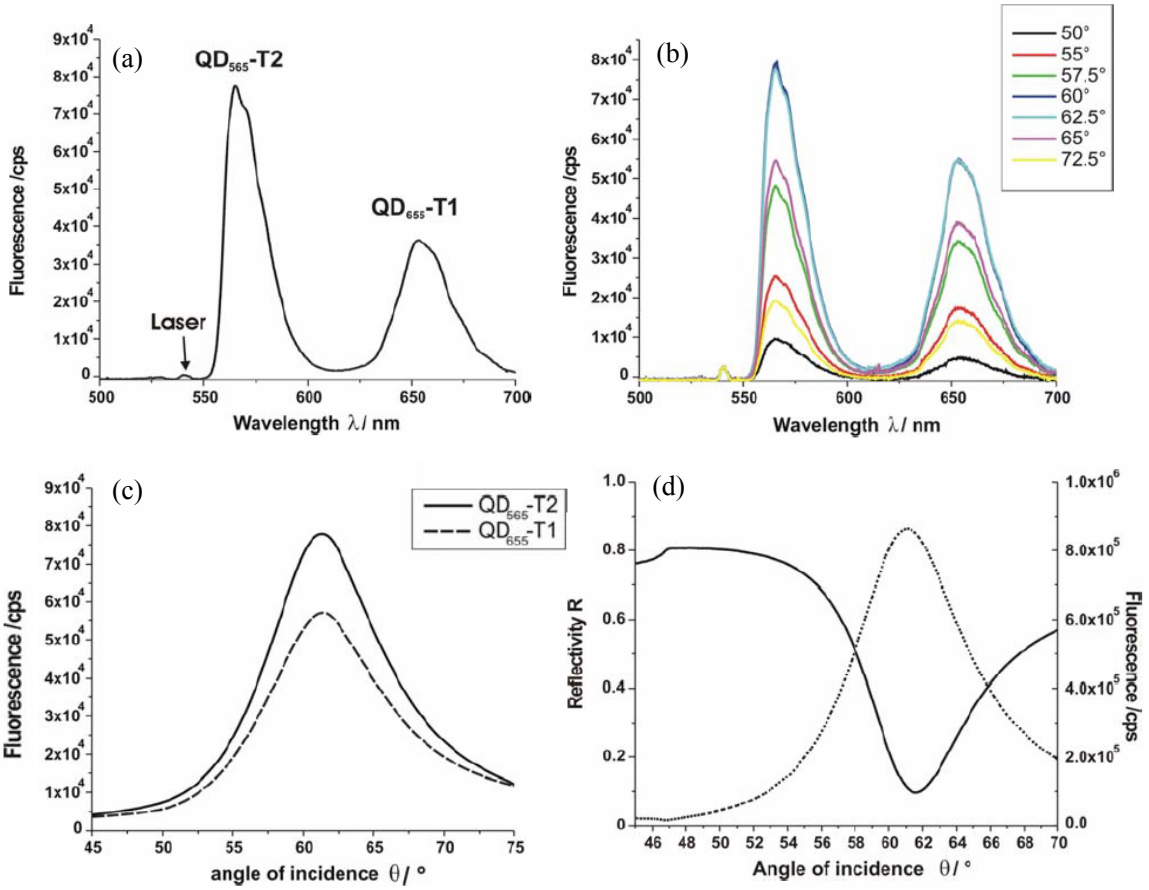

Figure 4.20: (a) Spectral resolution of the fluorescence signal generated by the surface hybridized QD_{565}-T2 / QD_{655}-T1 quantum dot mixture (injection time 10min); (b) Some of the spectrally resolved surface plasmon enhanced fluorescence spectra taken during an angular scan from θ = 45° to θ = 75° in Δθ = 2.5°; Derived from this data (c) shows two fluorescence intensity angle scans of QD_{565}-T2 and QD_{655}-T1, respectively; In comparison (d) shows the reflectivity (solid line) and fluorescence intensity (dashed line) achieved from a SPFS angle scan of QD_{655}-T1 hybridized to a P1 loaded sensor surface.

4.5.3.7. Conclusions and outlooks

The presented study is the first demonstration of an analytical combination of surface plasmon enhanced fluorescence spectroscopy with a fluorescent analyte tagged by semiconducting nanocrystals. These quantum dots show several advantages compared to the classic organic dyes, the most important one being their broad spectral

absorption range and the well defined sharp emission wavelength, which makes it possible to excite several quantum dot populations simultaneously with a single light source and, hence, at a single angle of incidence for resonance surface plasmon excitation.

Our experiments showed clearly, that a conjugation system consisting of 5-biotin tagged single stranded DNA sequences attached to streptavidin couple CdSe/ZnS core shell quantum dots is suitable for analyte detection by SPR and SPFS. The specific hybridization of QD conjugated DNA-single stands to sensor attached complementary sequences could be detected by a substantial shift in the angular reflectivity spectrum of the SPR, as well as, by a high fluorescence signal, originating from the DNA bound QDs.

The transfer of the system to the platform of surface plasmon enhanced fluorescence microscopy and the organization of the catcher probe DNA in a micro array format rendered a qualitative analytical approach of measuring the decomposition of QDx-DNAy mixtures possible. The spectral resolution of the obtained multicolor images with a spectrograph shows the potential of the combination of QD-DNA conjugates with SPFS for future applications in DNA chip analytics.

The results obtained so far are very promising, indicating great potential both for fundamental studies and for practical applications in biosensor development. There is no doubt that more investigations will be conducted in the future. The next step will be extending these SPS fluorescence techniques to the multi-protein multi-DNA analysis. We are expecting to give the detailed information of surface reaction quantitatively and visually.

Bibiology:

1. Lowe, C. R. An introduction to the concepts and technology of biosensors. *Biosensors* **1**, 3-16 (1985)
2. Turner, A. P. F., Karube, I. & Wilson, G. S. *Biosensors: Fundamentals and applications* (Oxford University Press, New York, 1987)
3. Buckle, M., Williams, R. M., Negroni, M, & Buc, H. *Proc. Natl. Acd. Sci. USA* **93**, 889-894 (1996)
4. Ligler, F. S. & Rabbany, S. Y. in *Synthetic microstructures in biological research* 67-75 (Plenum Press, New York, 1992)
5. Hall, E. A. H. *Biosensors* (Springer, Heidelberg, 1990)
6. Buerk, D. G. *Biosensors* (Technomic Publishing AG, Lancaster, USA, 1992)
7. Guibault, G. G. & Schnidt, R. D. Electrochemical, piezoelectric and fibre-optic biosensors, *Biosensors* **1**, 257-289 (1991)
8. Raether, H. *Surface Plasmon on Smooth and Rough Surfaces and on Gratings* (Springer, Berlin, 1988)
9. Grahm, C. R., Leslie, D. & Squirell, D. J. *Biosensors and Bioelectronics* **7**, 487-493 (1992)
10. Piunno, P. A. E., Krull, U.J., Hudson, R. H. E., Damha, M. J. & Cohen, H. *Anal. Chem.* **67**, 2635-2643 (1995)
11. Abel, A. P., Weller, M. G., Duvuneck, G. L., Ehrat, M. & Widmer, W. *Anal. Chem.* **68**, 2905-2912 (1996)
12. Attridge, J. W., Daniels, P. B., Deacon, J. K., Robinson, G. A. & Davidson, G. P. Sensitivity enhancement of optical immunosensors by the use of a surface plasmon resonance fluoroimmunoassay. *Biosens Bioelectron* **6**, 201-14 (1991)
13. Liebermann, T. & Knoll, W. Surface-plasmon field-enhanced fluorescence spectroscopy. *Colloids and Surfaces a-Physicochemical and Engineering Aspects* **171**, 115-130 (2000)
14. Agranovich, V. M. *Surface polaritonos* (North Hollan, Amsterdam, 1982)
15. Yeh, P. *Optical Waves in Layered Media* (John Wiley & Sons, New York, 1988)
16. O'Donnel, C. M. & Suffin, S. c. Fluorescen Immunoassays. *Anal. Chem.* **51** (1979)
17. Chan, D. W. *Fluorescent Immunoassays: a practical guide* (Academic Press, San Diego, 1987)
18. Christopoulos, T. K. & Diamandis, E. P. *Immunoassay* (Academic Press, San Diego, 1996)
19. Smith, D. J. Enhancement fluoroimmunoassay of thyroxine. *FEBS. Lett.* **77** (1977)

20. Lin, M. & Nielsen, K. J. Binding of the Brucella abortus lipopolysaccharide O-chain fragment to a monoclonal antibody. Quantitative analysis by fluorescence quenching and polarization . *Bioconjugate Chem.* **4** (1997)

21. Chan, I. N., Lin, J. N., Andrade, J. d. & Herron, J. N. Photoaffinity Labeling of Antibodies for Application in Homogeneous Fluoroimmunoassays. *Anal. Chem.* **67** (1995)

22. Ullman, E. F., Schwarzberg, M. & Rubenstein, K. E. Fluorescent Excitation Transfer Immunoassay: A General Method for Determination of Agents. *J. Biol. Chem.* **251**, 4172-4178 (1976)

23. Lazowski, K. W. & Kaczmarek, L. Highly sensitive detection of hybridization of oligonucleotides to specific sequences of nucleic acids by application of fluorescence resonance energy transfer. *Antisense Nucleic Acid Drud Dev* **10 (2)**, 97-103 (20000

24. Lakowica, J. R. *Principles of Fluorescence Spectroscopy* (Plenum Press, New York, London, 1983)

25. Ludwig Boltzmann Studien über das Wärmegleichgewicht unter Gasmolekülen, *Wiener Berichte*, 66: 275–370 (1872)

26. Michael Kash Characterization of Electronic Transitions in Complex Molecules *Discuss. Faraday Soc.* 9, 14-19 (1950)

27. H. Kuhn, D. Mödius, H. Bücher, in: A. Weissberger and B. W. Rossiter (Eds.), Physical Methods of Chemistry, Wiley Interscience, New York, 1972, Part ⅢB, Chapter 7

28. Rothenhäusler, B., Knoll, W. *Nature* **171**, 615-617 (1988)

29. Hickel, W., Kamp, D., Knoll, W. *Nature* **339**,186-190 (1989)

30. Liebermann, T., Knoll, W. *Langmuir* **19**, 1567-1572 (2003)

31. Hickel, W., Knoll, W. *Thin Solid Films* **18**7, 349-356 (1990)

32. Liebermann, T.; Knoll, W. Surface-plasmon field-enhanced fluorescence spectroscopy. *Colloids Surf.*, A, **171** 115-130 (2000)

33. Chan, W. C. W., Maxwell, D. j., Gao, X., Bailey, R. E., Han, M. and Nie, S. *Cur. Op. Biotech.* **13**, 40-46 (2002)

34. Bruchez, J. R., Moronne, M., Gin, P., Weiss, S., Alivisatos, A. P. *Science* **281**, 2013-2015 (1998)